

See discussions, stats, and author profiles for this publication at: <https://www.researchgate.net/publication/26852389>

Monomeric and Oligomeric Amine–Borane σ -Complexes of Rhodium. Intermediates in the Catalytic Dehydrogenation of Amine–Boranes

ARTICLE in JOURNAL OF THE AMERICAN CHEMICAL SOCIETY · SEPTEMBER 2009

Impact Factor: 12.11 · DOI: 10.1021/ja906070r · Source: PubMed

CITATIONS

110

READS

31

5 AUTHORS, INCLUDING:



Andrew Weller

University of Oxford

177 PUBLICATIONS 3,224 CITATIONS

[SEE PROFILE](#)



Xinzhen Yang

Chinese Academy of Sciences

58 PUBLICATIONS 981 CITATIONS

[SEE PROFILE](#)



Michael B Hall

Texas A&M University

361 PUBLICATIONS 10,406 CITATIONS

[SEE PROFILE](#)

Monomeric and Oligomeric Amine–Borane σ -Complexes of Rhodium. Intermediates in the Catalytic Dehydrogenation of Amine–Boranes

Thomas M. Douglas,[†] Adrian B. Chaplin,[†] Andrew S. Weller,^{*,†} Xinzhen Yang,[‡] and Michael B. Hall^{*,‡}

Department of Chemistry, Inorganic Chemistry Laboratories, University of Oxford, Oxford OX1 3QR, U.K., and Department of Chemistry, Texas A&M University, College Station, Texas 77843

Received July 28, 2009; E-mail: andrew.weller@chem.ox.ac.uk; mbhall@tamu.edu

Abstract: A combined experimental/quantum chemical investigation of the transition metal-mediated dehydrocoupling reaction of $H_3B \cdot NMe_2H$ to ultimately give the cyclic dimer $[H_2BNMe_2]_2$ is reported. Intermediates and model complexes have been isolated, including examples of amine–borane σ -complexes of Rh(I) and Rh(III). These come from addition of a suitable amine–borane to the crystallographically characterized precursor $[Rh(\eta^6-1,2-F_2C_6H_4)(P^iBu_3)_2][BAr^F_4]$ [$Ar^F = 3,5-(CF_3)_2C_6H_3$]. The complexes $[Rh(\eta^2-H_3B \cdot NMe_2)(P^iBu_3)_2][BAr^F_4]$ and $[Rh(H)_2(\eta^2-H_3B \cdot NHMe_2)(P^iBu_3)_2][BAr^F_4]$ have also been crystallographically characterized. Other intermediates that stem from either H_2 loss or gain have been characterized in solution by NMR spectroscopy and ESI-MS. These complexes are competent in the catalytic dehydrocoupling (5 mol %) of $H_3B \cdot NMe_2H$. During catalysis the linear dimer amine–borane $H_3B \cdot NMe_2BH_2 \cdot NHMe_2$ is observed which follows a characteristic intermediate time/concentration profile. The corresponding amine–borane σ -complex, $[Rh(P^iBu_3)_2(\eta^2-H_3B \cdot NMe_2BH_2 \cdot NHMe_2)][BAr^F_4]$, has been isolated and crystallographically characterized. A Rh(I) complex of the final product, $[Rh(P^iBu_3)_2(\eta^2-(H_2BNMe_2)_2)][BAr^F_4]$, is also reported, although this complex lies outside the proposed catalytic cycle. DFT calculations show that the first proposed dehydrogenation step, to give $H_2B=NMe_2$, proceeds via two possible routes of essentially the same energy barrier: BH or NH activation followed by NH or BH activation, respectively. Subsequent to this, two possible low energy routes that invoke either $H_2/H_2B=NMe_2$ loss or $H_2B=NMe_2/H_2$ loss are suggested. For the second dehydrogenation step, which ultimately affords $[H_2BNMe_2]_2$, a number of experimental observations suggest that a simple intramolecular route is not operating: (i) the isolated complex $[Rh(P^iBu_3)_2(\eta^2-H_3B \cdot NMe_2BH_2 \cdot NHMe_2)][BAr^F_4]$ is stable in the absence of amine–boranes; (ii) addition of $H_3B \cdot NMe_2BH_2 \cdot NHMe_2$ to $[Rh(P^iBu_3)_2(\eta^2-H_3B \cdot NMe_2BH_2 \cdot NHMe_2)][BAr^F_4]$ initiates dehydrocoupling; and (iii) $H_2B=NMe_2$ is also observed during this process.

1. Introduction

The coordination chemistry of amine–boranes, prototypically $H_3B \cdot NH_3$, and their subsequent reactivity is an area of significant contemporary interest. This comes from the role that metal complexes play in controlling kinetics and product distributions for subsequent dehydrocoupling reactions to form linear or cyclic oligomers and polymers alongside the concomitant release of H_2 . Control of these processes has relevance to chemical hydrogen storage¹ and the synthesis of new main-group polymeric materials.² Transition metal catalysts utilized for dehydrogenation include Cp_2Ti derivatives,^{3,4} Re-nitrosyls,⁵ Ir-pincer complexes,^{6–8} Ru–amino complexes,^{9,10} and Cu/Ni-

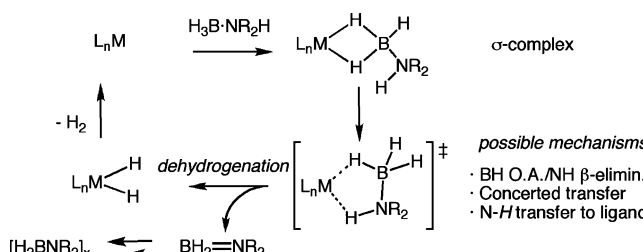
NHC complexes.¹¹ Colloidal-Rh has also been shown to be an active catalyst,^{12,13} for which in situ EXAFS suggests that the

- (4) Pun, D.; Lobkovsky, E.; Chirik, P. *J. Chem. Commun.* **2007**, 3297–3299.
- (5) Jiang, Y.; Berke, H. *Chem. Commun.* **2007**, 3571–3573.
- (6) (a) Dietrich, B. L.; Goldberg, K. I.; Heinekey, D. M.; Autrey, T.; Linehan, J. C. *Inorg. Chem.* **2008**, 47, 8583–8585. (b) Rousseau, R.; Schenter, G. K.; Fulton, J. L.; Linehan, J. C.; Engelhard, M. H.; Autry, T. *J. Am. Chem. Soc.* **2009**, 131, 10516–10524.
- (7) Hebden, T. J.; Denney, M. C.; Pons, V.; Piccoli, P. M. B.; Koetzle, T. F.; Schultz, A. J.; Kaminsky, W.; Goldberg, K. I.; Heinekey, D. M. *J. Am. Chem. Soc.* **2008**, 130, 10812–10820.
- (8) Denney, M. C.; Pons, V.; Hebden, T. J.; Heinekey, D. M.; Goldberg, K. I. *J. Am. Chem. Soc.* **2006**, 128, 12048–12049.
- (9) Kass, M.; Friedrich, A.; Drees, M.; Schneider, S. *Angew. Chem., Int. Ed.* **2009**, 48, 905–907.
- (10) Blacquiere, N.; Diallo-Garcia, S.; Gorelsky, S. I.; Black, D. A.; Fagnou, K. *J. Am. Chem. Soc.* **2008**, 130, 14034–14045.
- (11) Keaton, R. J.; Blacquiere, J. M.; Baker, R. T. *J. Am. Chem. Soc.* **2007**, 129, 1844–1845.
- (12) Jaska, C. A.; Manners, I. *J. Am. Chem. Soc.* **2004**, 126, 9776–9785.
- (13) Jaska, C. A.; Temple, K.; Lough, A. J.; Manners, I. *J. Am. Chem. Soc.* **2003**, 125, 9424–9434.
- (14) Fulton, J. L.; Linehan, J. C.; Autrey, T.; Balasubramanian, M.; Chen, Y.; Szymczak, N. K. *J. Am. Chem. Soc.* **2007**, 129, 11936–11949.

[†] University of Oxford.

[‡] Texas A&M University.

- (1) (a) Marder, T. B. *Angew. Chem., Int. Ed.* **2007**, 46, 8116–8118. (b) Stephens, F. H.; Pons, V.; Baker, R. T. *Dalton Trans.* **2007**, 2613–2626. (c) Hamilton, C. W.; Baker, R. T.; Staubitz, A.; Manners, I. *Chem. Soc. Rev.* **2009**, 38, 279–293.
- (2) Clark, T. J.; Lee, K.; Manners, I. *Chem.–Eur. J.* **2006**, 12, 8634–8648.
- (3) Clark, T. J.; Russell, C. A.; Manners, I. *J. Am. Chem. Soc.* **2006**, 128, 9582–9583.

Scheme 1. Inner Sphere Dehydrogenation Mechanism

active species might actually be smaller Rh_4 clusters.¹⁴ Transition-metal-mediated hydrolytic decomposition of amine–boranes and their derivatives has also been reported.¹⁵

Recent insight into the role of the metal complex in these transformations has revealed two possible general pathways for dehydrogenation. The first is *inner sphere*, in which the amine–borane coordinates to the metal center and undergoes H-transfer reactions aided by the metal by a variety of mechanistic steps. Scheme 1 illustrates one plausible reaction pathway for homogeneous systems that involves inner sphere dehydrogenation, although exact details of the mechanism are still being debated. Computational and experimental studies indicate a number of mechanistic scenarios for the dehydrogenation step depending on the metal/ligand combination: NH proton transfer to a coordinated ligand followed by transfer to the metal (Ni-N-heterocyclic carbene),¹⁶ intermolecular stepwise transfer of NH then BH (Cp_2Ti -derivatives),¹⁷ and concerted NH/BH activation at the metal center (Ir-pincer complexes).¹⁸ Oxidative addition of the BH bond followed by NH β -elimination has also been suggested.¹¹ All these routes implicate α -complexes of amine–boranes as intermediates in the reaction.¹⁹ The other alternative mechanistic scenario is that afforded by bifunctional Ru catalysts that are suggested to work via an *outer-sphere* dehydrogenation mechanism similar to that invoked for transfer dehydrogenation of alcohols.^{9,10} The role of free, dissociated, ligand in nickel N-heterocyclic carbene systems has also been recently discussed.²⁰

Despite this intense recent interest, details of intermediate species remain scarce,^{4,8} although materials that represent catalyst deactivation products have been isolated.^{4,7,8} The coordination chemistry of σ -amine–borane or phosphine–borane complexes has been developed over the past decade by Shimoji and co-workers and includes examples of group 6, 7, and 8 metals,^{21–25} but as far as we are aware there is only a brief

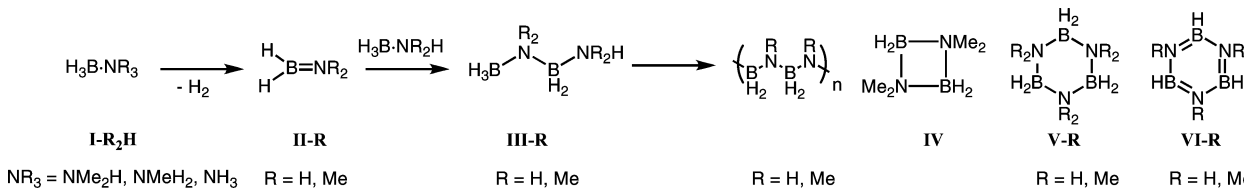
- (15) For leading references see. (a) Yoon, C. W.; Sneddon, L. G. *J. Am. Chem. Soc.* **2006**, *128*, 13992–13993. (b) Yan, J. M.; Zhang, X. B.; Han, S.; Shiota, H.; Xu, Q. *Angew. Chem., Int. Ed.* **2008**, *47*, 2287–2289.
- (16) (a) Yang, X. Z.; Hall, M. B. *J. Am. Chem. Soc.* **2008**, *130*, 1798–1799. (b) Yang, X. Z.; Hall, M. B. *J. Organomet. Chem.* **2009**, *694*, 2831–2838.
- (17) Luo, Y.; Ohno, K. *Organometallics* **2007**, *26*, 3597–3600.
- (18) Paul, A.; Musgrave, C. B. *Angew. Chem., Int. Ed.* **2007**, *46*, 8153–8156.
- (19) We define a σ borane complex as one having an intermolecular interaction between a B–H bond in a neutral ligand and a metal center. It encompasses three and four coordinate borane species. Anionic dihydridoborate and borohydride ligands are also known: Kubas, G. J. *Metal Dihydrogen and σ -Bond Complexes*; Kluwer Academic/Plenum Publishers: New York, 2001.
- (20) Zimmerman, P. M.; Paul, A.; Zhang, Z. Y.; Musgrave, C. B. *Angew. Chem., Int. Ed.* **2009**, *48*, 2201–2205.
- (21) Shimoji, M.; Nagai, S.; Ichikawa, M.; Kawano, Y.; Katoh, K.; Uruichi, M.; Ogin, H. *J. Am. Chem. Soc.* **1999**, *121*, 11704–11712.
- (22) Kakizawa, T.; Kawano, Y.; Shimoji, M. *Organometallics* **2001**, *20*, 3211–3213.

report of such species involvement in catalytic dehydrocoupling reactions.²⁶ There are no reported examples of group 9 complexes, although chelated systems of group 9 metals, related to those with agostic C–H interactions,²⁷ have been reported,^{28–31} as have dihydridoborate complexes.³² Related σ -complexes of three coordinate boron have also been synthesized.^{33–37} The valence isoelectronic relationship between amine–boranes and alkanes²⁵ means that the coordination chemistry of σ -amine–borane ligands also models that of transient transition-metal–alkane complexes observed in solution.³⁸

Experimental and computational work on the mechanism of transition-metal mediated dehydrocoupling of amine–boranes indicate complex processes that are dependent on functionalization patterns on the amine–borane and the identity of the metal center used.^{1c,40} For example, when using $H_3B \cdot NH_3$ with Rh,¹³ Ti,⁴ and Ni-based¹¹ systems, cyclic trimers and cross-linked derivatives result (e.g., **V-R** and **VI-R**, Scheme 2), Ir-pincer complexes give pentamers,⁸ and bifunctional Ru catalysts give poorly defined polymeric material.⁹ With $H_3B \cdot NMMe_2$, polymerization/oligomerization/trimerization is reported,^{6,10,13,41}

- (23) Yasue, T.; Kawano, Y.; Shimoji, M. *Angew. Chem., Int. Ed.* **2003**, *42*, 1727–1730.
- (24) Kawano, Y.; Hashiba, M.; Shimoji, M. *Organometallics* **2006**, *25*, 4420–4426.
- (25) Kawano, Y.; Yamaguchi, K.; Miyake, S. Y.; Kakizawa, T.; Shimoji, M. *Chem.—Eur. J.* **2007**, *13*, 6920–6931.
- (26) Shimoji, M.; Kawano, Y.; Taeko, T. S. Presented at the 224th ACS National Meeting, Boston, 2002.
- (27) Brookhart, M.; Green, M. L. H.; Parkin, G. *Proc. Natl. Acad. Sci. U.S.A.* **2007**, *104*, 6908–6914.
- (28) Macias, R.; Rath, N. P.; Barton, L. *Angew. Chem., Int. Ed.* **1999**, *38*, 162–164.
- (29) Ingleson, M.; Patmore, N. J.; Ruggiero, G. D.; Frost, C. G.; Mahon, M. F.; Willis, M. C.; Weller, A. S. *Organometallics* **2001**, *20*, 4434–4436.
- (30) (a) Bajko, Z.; Daniels, J.; Gudat, D.; Hap, S.; Nieger, M. *Organometallics* **2002**, *21*, 5182–5189. (b) Rankin, M. A.; MacLean, D. F.; McDonald, R.; Ferguson, M. J.; Lumsden, M. D.; Stradiotto, M. *Organometallics* **2009**, *28*, 74–83.
- (31) Wagler, J.; Hill, A. F. *Organometallics* **2008**, *27*, 2350–2353.
- (32) Westcott, S. A.; Marder, T. B.; Baker, R. T.; Harlow, R. L.; Calabrese, J. C.; Lam, K. C.; Lin, Z. *Polyhedron* **2004**, *23*, 2665–2677.
- (33) For examples of three coordinate boron σ complexes:(a) Muhoro, C. N.; He, X.; Hartwig, J. F. *J. Am. Chem. Soc.* **1999**, *121*, 5033–5046. (b) Hartwig, J. F.; Muhoro, C. N.; He, X.; Eisenstein, O.; Bosque, R.; Maseras, F. *J. Am. Chem. Soc.* **1996**, *118*, 10936–10937. (c) Montiel-Palma, V.; Lumbières, M.; Donnadieu, B.; Sabo-Etienne, S.; Chaudret, B. *J. Am. Chem. Soc.* **2002**, *124*, 5624–5625. (d) Crestani, M. G.; Munoz-Hernandez, M.; Arevalo, A.; Acosta-Ramirez, A.; Garcia, J. J. *J. Am. Chem. Soc.* **2005**, *127*, 18066–18073. (e) Alcaraz, G.; Helmstedt, U.; Clot, E.; Vendier, L.; Sabo-Etienne, S. *J. Am. Chem. Soc.* **2008**, *130*, 12878–12879. (f) Hebden, T. J.; Denney, M. C.; Pons, V.; Piccoli, P. M. B.; Koetzle, T. F.; Schultz, A. J.; Kaminsky, W.; Goldberg, K. I.; Heinekey, D. M. *J. Am. Chem. Soc.* **2008**, *130*, 10812–10820.
- (34) (a) Lachaize, S.; Essalah, K.; Montiel-Palma, V.; Vendier, L.; Chaudret, B.; Barthelat, J.-C.; Sabo-Etienne, S. *Organometallics* **2005**, *24*, 2935–2943. (b) Hartwig, J. F.; Cook, K. S.; Hapke, M.; Incarvito, C. D.; Fan, Y.; Webster, C. E.; Hall, M. B. *J. Am. Chem. Soc.* **2005**, *127*, 2538–2552.
- (35) Alcaraz, G.; Clot, E.; Helmstedt, U.; Vendier, L.; Sabo-Etienne, S. *J. Am. Chem. Soc.* **2007**, *129*, 8704–8705.
- (36) Lam, W. H.; Shimada, S.; Batsanov, A. S.; Lin, Z.; Marder, T. B.; Cowan, J. A.; Howard, J. A. K.; Mason, S. A.; McIntyre, G. J. *Organometallics* **2003**, *22*, 4557–4568.
- (37) Hesp, K. D.; Rankin, M. A.; McDonald, R.; Stradiotto, M. *Inorg. Chem.* **2008**, *47*, 7471–7473.
- (38) Lawes, D. J.; Geftakis, S.; Ball, G. E. *J. Am. Chem. Soc.* **2005**, *127*, 4134–4135.
- (39) Zimmerman, P. M.; Paul, A.; Zhang, Z. Y.; Musgrave, C. B. *Inorg. Chem.* **2009**, *48*, 1069–1081.
- (40) Pons, V.; Baker, R. T.; Szymbczak, N. K.; Heldebrand, D. J.; Linehan, J. C.; Matus, M. H.; Grant, D. J.; Dixon, D. A. *Chem. Commun.* **2008**, 6597–6599.

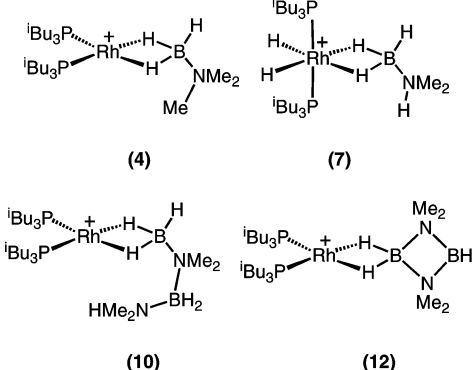
Scheme 2. Abridged Dehydrogenation and Dehydrocoupling Reaction Scheme for Amine–Boranes and the Suggested Involvement of Linear Dimer **III–R**^{17,18,39,40}



while $\text{H}_3\text{B}\cdot\text{NMe}_2\text{H}$ gives the cyclic dimer $[\text{H}_2\text{BNMe}_2]_2$ (**IV**).^{3,4,13,14,42,43} Detailed computational^{16–18,20,39} and experimental studies⁴⁰ suggest that metal-mediated dehydrogenation leads first to amino–boranes, $\text{H}_2\text{B}=\text{NR}_2$ (**II–R**, Scheme 2), which then dimerize or oligomerize to eventually form the observed products. In some cases the formation of the linear dimer $\text{H}_3\text{B}\cdot\text{NR}_2\text{BH}_2\cdot\text{NR}_3\text{H}$ (**III–R**) is suggested as an early step in these processes, which can come from reaction of $\text{H}_2\text{B}=\text{NR}_2$ with $\text{H}_3\text{B}\cdot\text{NHR}_2$.^{13,39,40} Such a compound, which could be bound to a metal or generated free under the reaction conditions, could then proceed to give the final products via further dehydrocoupling pathways. The role of metal in this process has not been firmly established, although the catalytic dehydrocoupling of **III–Me** using colloidal Rh to form dimeric $[\text{H}_2\text{BNMe}_2]_2$ has been reported previously by Manners and co-workers demonstrating its possible role as an intermediate.¹³ However, details of both the coordination chemistry of **III–Me** and the role that the metal plays in its dehydrogenation have not been reported. Related calcium complexes of the $[\text{HNHB}-\text{NHBH}]^{2-}$ dianion result from the reaction of calcium hydrides with $\text{H}_3\text{B}\cdot\text{NH}_3$.⁴⁴ Manners and co-workers have shown that the catalytic dehydrocoupling of $\text{H}_3\text{B}\cdot\text{PPh}_2\text{H}$ using Rh(I) precatalysts gives $\text{H}_3\text{B}\cdot\text{PPh}_2\text{BH}_2\cdot\text{PPh}_2\text{H}$ at 90 °C and the cyclic products $[\text{Ph}_2\text{PBH}_2]_3$ and $[\text{Ph}_2\text{PBH}_2]_4$ at 120 °C. Monitoring this higher temperature reaction shows a mixture of $\text{H}_3\text{B}\cdot\text{PPh}_2\text{BH}_2\cdot\text{PPh}_2\text{H}$ and the cyclic species, suggesting the possible role of the linear oligomer as an intermediate.⁴⁵

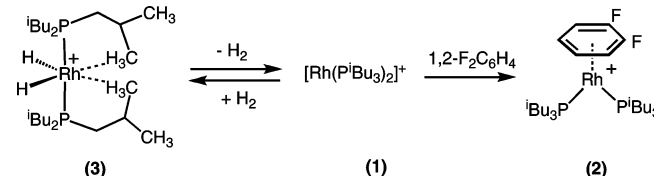
As metal σ -complexes are implicated throughout the catalytic cycle in inner-sphere mechanisms we have set out to deliberately synthesize such species and study their coordination chemistry and onward reactivity. Here we report upon the synthesis of σ -complexes of a variety of amine–boranes based upon $\text{H}_3\text{B}\cdot\text{NMe}_2\text{H}$ complexed with rhodium (Scheme 3) that are either suggested as putative intermediates in the catalytic dehydrocoupling or model complexes thereof. The approach we use is to take a preformed cationic low-coordinate latent-“12-electron” $[\text{Rh}(\text{P}^{\text{i}}\text{Bu}_3)_2]^+$ fragment with suitable amine–borane ligands. Utilizing density functional theory (DFT), we also report on computational work that evaluates possible mechanistic routes in the dehydrocoupling of $\text{H}_3\text{B}\cdot\text{NHMe}_2$ to give $\text{H}_2\text{B}=\text{NMe}_2$ using these Rh systems (i.e., **I** to **II**). Although none of the systems reported herein offer improvement on the current best, in terms of turnover frequency for the dehydrocoupling,^{8–10} this attenuated reactivity has the benefit of allowing for intermediates to be observed and thus gives insight

Scheme 3. Representative Complexes Reported in This Paper^a



^a $[\text{BAR}_4^{\text{F}}]^-$ anions are not shown.

Scheme 4. Synthesis of the Precursor Complexes **1–3**^a



^a $[\text{BAR}_4^{\text{F}}]^-$ anions are not shown.

into mechanistic processes. Aspects of this work have been communicated.⁴³

2. Results and Discussion

2.1. Synthesis of σ -Complexes of $\text{H}_3\text{B}\cdot\text{NMe}_3$ and $\text{H}_3\text{B}\cdot\text{NMMe}_2$. We have previously reported upon the synthesis of the latent 12-electron complex $[\text{Rh}(\text{P}^{\text{i}}\text{Bu}_3)_2][\text{BAR}_4^{\text{F}}]$ **1** (Scheme 4, $\text{Ar}^{\text{F}} = \text{C}_6\text{H}_3(\text{CF}_3)_2$) from straightforward H_2 removal from the 14-electron complex $[\text{Rh}(\text{H})_2(\text{P}^{\text{i}}\text{Bu}_3)_2][\text{BAR}_4^{\text{F}}]$ **3**. For **3** a crystal structure showed that the coordinate and electronic unsaturation is relieved by supporting agostic C–H interactions,⁴⁶ and this structure is supported by DFT calculations (Figure 1). Such interactions are also probably present in **1** in the solid state, and the calculated structure shows two such $\text{Rh}\cdots\text{H}_3\text{C}$ contacts trans to the phosphines (Figure 1) making a pseudo-square planar Rh(I) species. Noteworthy is that the trans isomer of **1** is 3.1 kcal/mol less stable than the cis (gas phase free energy). Both these complexes are well set up for coordination of weak ligands such as amine–boranes as the agostic interactions stabilize a latent coordination site. **1** reacts with weak ligands such as dichloroethane or fluorobenzene, to form a simple adduct and an η^6 -arene complex, respectively.⁴⁶ In this contribution the even weaker solvent 1,2-difluorobenzene is the solvent of choice for the study of the

- (41) Staubitz, A.; Soto, A. P.; Manners, I. *Angew. Chem., Int. Ed.* **2008**, *47*, 6212–6215.
- (42) Sloan, M. E.; Clark, T. J.; Manners, I. *Inorg. Chem.* **2009**, *48*, 2429–2435.
- (43) Douglas, T. M.; Chaplin, A. B.; Weller, A. S. *J. Am. Chem. Soc.* **2008**, *130*, 14432–14433.
- (44) Spielmann, J.; Jansen, G.; Bandmann, H.; Harder, S. *Angew. Chem., Int. Ed.* **2008**, *47*, 6290–6295.
- (45) Dorn, H.; Singh, R. A.; Massey, J. A.; Nelson, J. M.; Jaska, C. A.; Lough, A. J.; Manners, I. *J. Am. Chem. Soc.* **2000**, *122*, 6669–6678.

- (46) Douglas, T. M.; Chaplin, A. B.; Weller, A. S. *Organometallics* **2008**, *27*, 2918–2921.

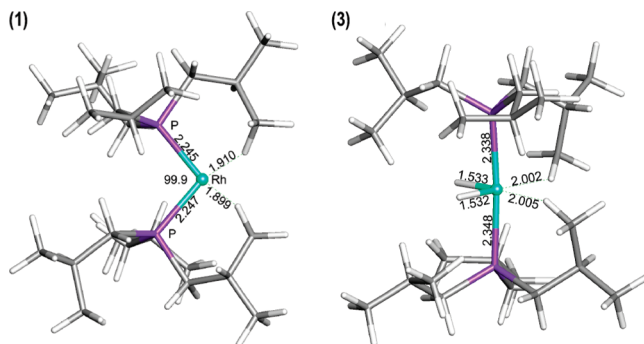


Figure 1. DFT optimized structures of the cationic portions of **1** and **3**. Bond lengths in Å. Bond angle in degrees.

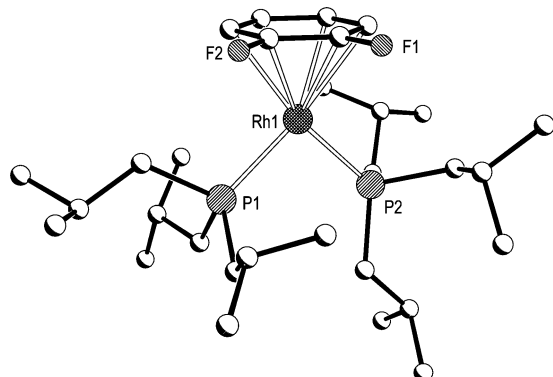


Figure 2. Molecular structure the cationic portion of **2**: ball and stick diagram. Minor disordered components and H atoms omitted for clarity.

isolation and reactivity of these sensitive complexes, which decompose slowly in CH_2Cl_2 . Dissolving **1** in this solvent results in the corresponding η^6 -arene complex $[\text{Rh}(\eta^6\text{-1,2-}\text{F}_2\text{C}_6\text{H}_4)(\text{P}^i\text{Bu}_3)_2][\text{BAr}^{\text{F}}_4]$ **2**. As **2** represents the starting material generated *in situ* for all subsequent reactivity, we have characterized it by NMR spectroscopy, ESI-MS, and X-ray crystallography. The solid-state structure of **2**, although of low quality ($R_1 = 9\%$), demonstrates that the 1,2-fluorobenzene ligand coordinates η^6 , similar to that observed for $[\text{Rh}(\eta^6\text{-FC}_6\text{H}_5)(\text{P}^i\text{Bu}_3)_2][\text{BAr}^{\text{F}}_4]$ ⁴⁶ (Figure 2). The NMR data for **2** in 1,2- $\text{F}_2\text{C}_6\text{H}_4$ solution are in full accord with the structure, although the coordinated arene resonances were obscured by the protio solvent. Dissolving crystals of **2** in alternate solvents results in the weakly bound arene ligand being displaced; for example, in 1,2-dichloroethane the resulting adduct complex is formed (Supporting Information).⁴⁶ As far as we are aware **2** is the first example of a complex coordinated with 1,2-difluorobenzene⁴⁷ and is also a rare example of a fluoroarene complex of a late transition metal.^{48,49} Complex **2** is an excellent source of a latent 12-electron $[\text{Rh}(\text{P}^i\text{Bu}_3)_2]^+$ fragment and is well set up for reaction with amine–boranes, which is discussed next.

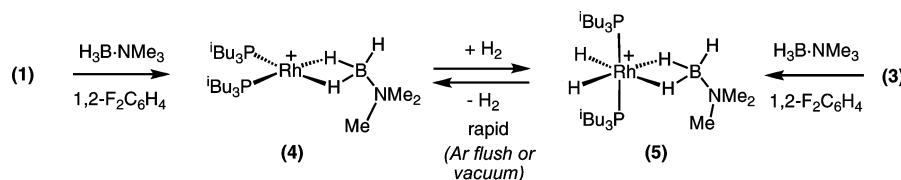
- (47) Complexes of 1,2-iodoarenes are known, for example: Crabtree, R. H.; Faller, J. W.; Mellea, M. F.; Quirk, J. M. *Organometallics* **1982**, *1*, 1361–1366.
- (48) (a) Douglas, T. M.; Notre, J. L.; Brayshaw, S. K.; Frost, C. G.; Weller, A. S. *Chem. Commun.* **2006**, 3408–3410. (b) Palacios, M. D.; Puerta, M. C.; Valerga, P.; Lledos, A.; Veilly, E. *Inorg. Chem.* **2007**, *46*, 6958–6967. (c) Willems, S. T. H.; Budzelaar, P. H. M.; Moonen, N. N. P.; de Gelder, R.; Smits, J. M. M.; Gal, A. W. *Chem. Eur. J.* **2002**, *8*, 1310–1320.
- (49) Douglas, T. M.; Brayshaw, S. K.; Dallanegra, R.; Kociok-Kohn, G.; Macgregor, S. A.; Moxham, G. L.; Weller, A. S.; Wondimagegn, T.; Vadivelu, F. *Chem.—Eur. J.* **2008**, *14*, 1004–1022.

As the dehydrocoupling of amine–boranes may proceed via B–H/N–H activation for inner sphere and outer sphere reactions (in whatever order), in the anticipation of first isolating a moderately stable amine–borane σ -complex, $\text{H}_3\text{B}\cdot\text{NMe}_3$ was used initially, in which the quaternary nitrogen offers no protic hydrogen. Metal complexes from groups 6,²¹ 7,²⁵ and 8²⁴ of $\text{H}_3\text{B}\cdot\text{NMe}_3$, as well as closely related complexes, have previously been reported by Shimoj and co-workers, but no later transition metal complexes are known.

Addition of $\text{H}_3\text{B}\cdot\text{NMe}_3$ to a 1,2- $\text{F}_2\text{C}_6\text{H}_4$ solution of **2** (generated *in situ* from **1**) results in an immediate color change from orange to deep purple. NMR data, ESI-MS, and a solid-state structure identify this new product as $[\text{Rh}(\eta^2\text{-H}_3\text{B}\cdot\text{NMe}_3)(\text{P}^i\text{Bu}_3)_2][\text{BAr}^{\text{F}}_4]$ **4** (Scheme 5). Air- and temperature-sensitive crystals were grown from 1,2- $\text{F}_2\text{C}_6\text{H}_4$ /pentane solvent in excellent isolated yield (87%), and the solid-state molecular structure is shown in Figure 3. The amine–borane ligand is η^2 -coordinated through two Rh–H–B σ -bonds, and the Rh(I) center is pseudo square planar: the sum of angles around Rh1 = 360.3°. The hydrogen atoms associated with the boron B1 (H1A, H1B, H1C) were located on the Fourier difference map. The Rh–B distance, 2.180(4) Å, is longer than a Rh–B boryl, namely, $(^i\text{Pr}_3\text{P})_2\text{RhHCl}(\text{BO}_2\text{C}_6\text{H}_4)$ [1.965(2) Å]³⁶ and $(\text{PMe}_3)_4\text{Rh}(\text{BO}_2\text{C}_6\text{H}_4)$ [2.047(2) Å].⁵⁰ It is significantly shorter than that observed in the Rh(I) chelated complexes $[\text{Rh}(\text{cod})(\eta^2\text{-H}_3\text{B}\cdot\text{PPh}_2\text{CH}_2\text{PPh}_2)][\text{BPh}_4]$ [2.313(3) Å]²⁹ and $\text{Rh}(\text{PPh}_3)_2(\eta^2\text{-H}_3\text{B-7-azaindol-7-ylborate})$ ³¹ but very similar to that observed in the Rh(I) dihydridoborate complex $\text{Rh}(\eta^2\text{-H}_2\text{BC}_8\text{H}_{14})(\text{P}^i\text{Pr}_3)_2$ [2.170(2) Å]³² and the chlorohydridoborates $\text{RuCp}^*(\text{PMe}_3)(\eta^2\text{-BH}_3\text{Cl})$ [2.122(8) Å]⁵¹ and $\text{RuCp}^*(\text{P}^i\text{Pr}_3)\text{-}(\text{BH}_2\text{MesCl})$ [2.162(3) Å].³⁷ Although within the experimental limits of the X-ray diffraction experiment (3σ) the bridging hydride ligands are not elongated compared to the terminal hydride [viz. 1.23(3) vs B1–H1C 1.05(4) Å], there does appear to be a trend that they become longer on coordination with the metal, while the acute H–Rh–H angle of 68(2)° points toward a complex that is best described as a Rh(I) center ligated with a σ -borane that has a significant Rh…B interaction, rather than an alternate Rh(III)-dihydride with a boryl ligand.^{34,52} The observation of a significantly quadrupolar broadened signal for the bridging hydrides in the ^1H NMR spectrum (fwhm = 210 Hz) also demonstrates a significant B–H interaction. The DFT calculated structure for **4** closely mirrors those experimentally observed in Figure 4.

In solution the $\text{H}_3\text{B}\cdot\text{NMe}_3$ ligand remains coordinated to the metal center, and ESI-MS shows a strong molecular ion at $m/z = 580.388$ (calcd 580.382). In addition to signals due to ^iBu and NMe_3 groups, the ^1H NMR spectrum at room temperature shows a quadrupolar broadened relative integral 3H signal at $\delta = -2.12$, which sharpens in the $^1\text{H}\{^{11}\text{B}\}$ NMR spectrum. This integral 3-H signal indicates rapid exchange between terminal and bridging hydrides at room temperature, as has been observed for both η^1 - σ -complexes^{21,22,24} and η^2 -chelated phosphine boranes.^{28,53,54} Cooling to 190 K arrests this fluxional process and results in the observation of a very broad, integral 2-H signal

- (50) Dai, C.; Stringer, G.; Marder, T. B.; Scott, A. J.; Clegg, W.; Norman, N. C. *Inorg. Chem.* **1997**, *36*, 272–273.
- (51) Kawano, Y.; Shimoj, M. *Chem. Lett.* **1998**, 935–936.
- (52) Hartwig, J. F.; De Gala, S. R. *J. Am. Chem. Soc.* **1994**, *116*, 3661–3662.
- (53) Merle, N.; Koicok-Kohn, G.; Mahon, M. F.; Frost, C. G.; Ruggerio, G. D.; Weller, A. S.; Willis, M. C. *Dalton Trans.* **2004**, 3883–3892.
- (54) Merle, N.; Frost, C. G.; Kociok-Kohn, G.; Willis, M. C.; Weller, A. S. *Eur. J. Inorg. Chem.* **2006**, 4068–4073.

Scheme 5. Synthesis of $\text{H}_3\text{B}\cdot\text{NMe}_3$ Complexes^a

^a $[\text{BAR}^{\text{F}}_4]^-$ anions are not shown.

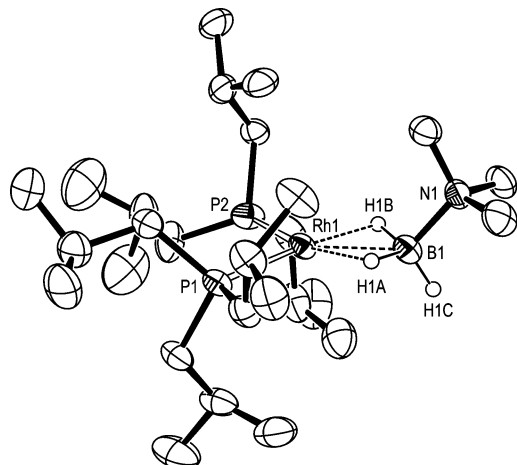


Figure 3. Molecular structure of the cationic portion of **4**: ellipsoids depicted at the 50% probably level. Minor disordered components and most H atoms omitted for clarity. Selected bond lengths (\AA) and angles (deg): Rh1–B1, 2.180(4); Rh1–P1, 2.2412(10); Rh1–P2, 2.2149(10); B1–N1, 1.594(5); Rh1–H1A, 1.80(4); Rh1–H1B, 1.84(4); B1–H1A, 1.23(3); B1–H1B, 1.23(3); B1–H1C, 1.05(4); P2–Rh1–P1, 97.35(4); P1–Rh1–B1, 135.18(11); P2–Rh1–B1, 126.99(11); N1–B1–Rh1, 129.2(3); Rh1–H1A–B1, 90(2); Rh1–H1B–B1, 88(2); H1A–Rh1–H1B, 68(2).

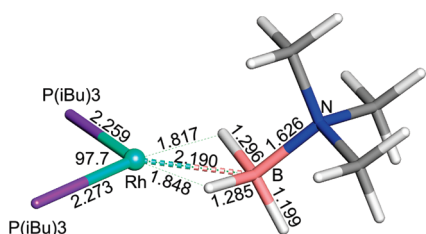


Figure 4. DFT optimized structure of the cationic portion of **4**. Bond lengths in \AA . Bond angle in degrees. The ^iBu groups are not shown for clarity.

at $\delta = -5.55$ assigned to the Rh–H–B protons, now consistent with the solid-state structure. We could not observe the corresponding terminal B–H proton, which is presumably broad and possibly obscured by the aliphatic phosphine protons. Exchange probably occurs by a $\eta^2\text{-}\eta^1\text{-}\eta^2$ process, as has been calculated for exchange in η^1 -amine–borane complexes⁵⁵ and also observed on the chemical time scale as hemilabile behavior in chelated systems.^{51,53,54} A single environment is observed in the $^{31}\text{P}\{^1\text{H}\}$ NMR spectrum that has a large coupling constant of 175 Hz consistent with a Rh(I) center. The ^{11}B NMR spectrum displays a broad signal at $\delta = 23.1$, shifted 30.4 ppm downfield from $\text{H}_3\text{B}\cdot\text{NMe}_3$, consistent with a significant Rh···B interaction.^{53,56} Table 1 shows that for all the compounds crystallographically characterized in this paper the ^{11}B chemical shifts move downfield significantly on coordination. The Rh(I) complexes (**4**, **10**, and **12**) show both shorter Rh···B interactions

Table 1. Comparison of Rh–B Bond Length, $\delta(^{11}\text{B})$ of Coordinated Boron, and the Chemical Shift Difference ($\Delta\delta$) Compared with Free Ligand^a

	Rh–B(\AA)	$\delta(^{11}\text{B})$	$\Delta\delta(^{11}\text{B})^*$
(4)	2.180(4)	23.1	30.4
(7)	2.318(8)	2.2	15.2
(10)	2.166(8)/2.202(9)	26.0	38.8
(12)	2.140(7)/2.161(6)	31.1	25.7

^a For the column marked with *, see Experimental Section for chemical shifts of free amine–boranes in 1,2-F₂C₆H₄ solvent.

and larger changes in chemical shift [$\Delta\delta(^{11}\text{B})$] compared to the Rh(III) example (**7**).

Complex **4** is stable in 1,2-F₂C₆H₄ solution, although it is very air-sensitive and best handled in an argon-filled glovebox. Addition of H₂ to complex **4** results in an immediate color change to yellow and the formation of the new complex [Rh(H)₂($\eta^2\text{-H}_3\text{B}\cdot\text{NMe}_3$)(P*i*Bu₃)₂][BAR^F₄] **5**. Complex **5** can also be prepared by addition of H₃B·NMe₃ to a 1,2-F₂C₆H₄ solution of **3** (Scheme 5). Complex **5** readily loses H₂ to re-form **4** and thus is best characterized under an atmosphere of H₂ (1 atm), by NMR spectroscopy and ESI-MS. These NMR data are very similar to that for the H₃B·NHMe₂ adduct (**7**) for which a single crystal X-ray structural determination shows an η^2 -coordinated amine–borane (vide infra). The presence of a Rh(III) center is indicated by a reduced ¹⁰⁵Rh–³¹P coupling constant compared with **4**, $\delta = 21.10$ [d, $J(\text{RhP})$ 106 Hz]. The ¹H NMR spectrum shows a sharp, integral 2-H doublet of triplets at $\delta = -18.81$ due to two equivalent hydride ligands, which becomes a doublet on ³¹P decoupling. These coupling patterns demonstrate that the hydrides are orientated cis to the phosphine ligands. A very broad quadrupolar-broadened relative integral 3-H signal at $\delta = -0.47$ is assigned to the B–H–Rh protons, indicating rapid site exchange for the B–H protons, which becomes less broad on decoupling ¹¹B. Cooling to 200 K did not freeze out the site exchange between terminal and bridging hydrides, perhaps suggesting a weaker Rh···H–B interaction which would be consistent with the strong trans influence of the hydrides (Table 1). The ¹¹B chemical shift also reflects this, with a very broad signal observed at $\delta = 5.1$ shifted considerably less downfield from free amine–borane compared with **4** (Table 1).

As a result of the ready H₂ loss, we have not been able to obtain crystalline material of **5**; however, inspection of a space-filling diagram of closely related **7** (Figure 5, vide infra) indicates that steric pressure of the trans-axial phosphines and the NMe₃ group could promote H₂ loss, favoring the pseudo-square-planar Rh(I) structure in **4**. This is not present in **7**, which does not lose H₂ as readily (vide infra). Addition of H₃B·NMe₃ to d₂–**3**, [Rh(D₂)(P*i*Bu₃)₂][BAR^F₄], under a partial pressure of D₂(g), resulted in a washing of deuterium into the B–H positions

(55) Kawano, Y.; Kakizawa, T.; Yamaguchi, K.; Shimoj, M. *Chem. Lett.* **2006**, 35, 568–569.

(56) Alcaraz, G.; Sabo-Etienne, S. *Coord. Chem. Rev.* **2008**, 252, 2395–2409.

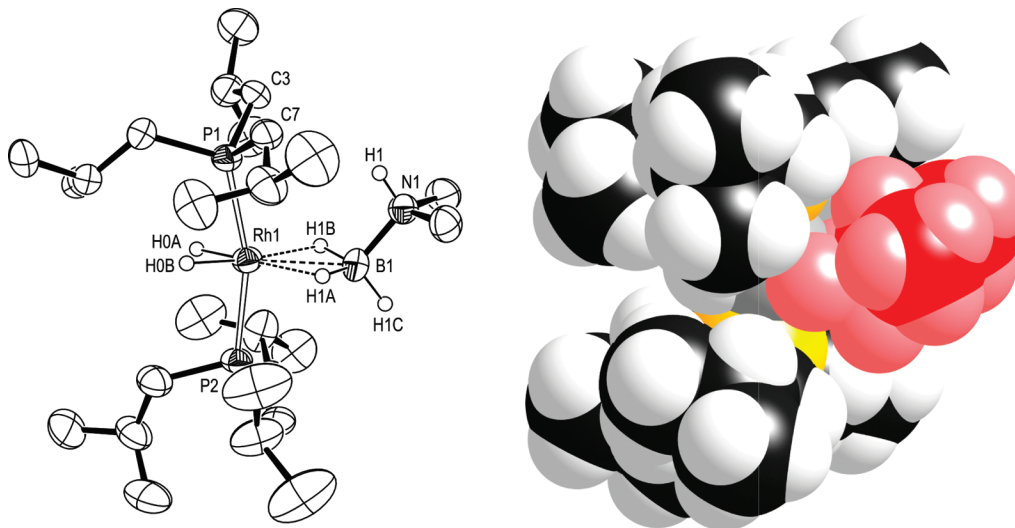
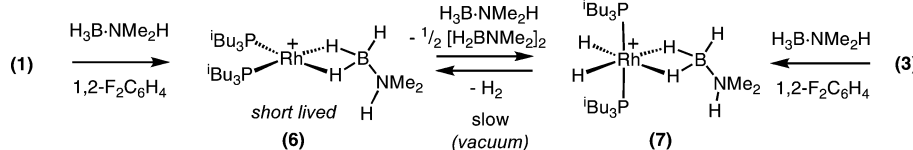


Figure 5. Molecular structure of the cationic portion of **7** (ellipsoids depicted at the 50% probably level, most H atoms omitted for clarity) and space filling diagram (van der Waals radii with $H_3B \cdot NHMe_2$ highlighted in red). Selected bond lengths (\AA) and angles (deg): Rh1–B1, 2.318(8); Rh1–P1, 2.307(2); Rh1–P2, 2.302(2); Rh1–HOA, 1.42(6); Rh1–HOB, 1.41(6); B1–N1, 1.595(10); Rh1–H1A, 1.82(6); Rh1–H1B, 1.86(7); B1–H1A, 1.20(4); B1–H1B, 1.20(4); B1–H1C, 1.10(7); H1–H3B, 2.47; H1–H7A, 2.88; P1–Rh1–P2, 163.65(7); P1–Rh1–B1, 103.6(2); P2–Rh1–B1, 92.6(2); Rh1–B1–N1, 125.1(5); Rh1–H1A–B1, 98(4); Rh1–H1B–B1, 96(4); H1A–Rh1–H1B, 61(3); H1A–B1–H1B, 104(5). H3B and H7A are placed in calculated positions.

Scheme 6. Synthesis of $H_3B \cdot NHMe_2$ Complexes^a



^a $[BAr^F_4]^-$ anions are not shown.

of **5** and hydrogen into the Rh-D positions. Dissolved H_2 and HD are observed [δ 4.60; δ 4.56 $J(HD)$ 42 Hz, respectively]. These observations suggest reversible B–H activation at the metal center, and we suggest that this is most likely via a Rh(I) complex such as **4** rather than a Rh(III) dihydride **5** as this invokes a Rh(I)/Rh(III) couple rather than a Rh(III)/Rh(V). This is supported by the rather low calculated B–H bond activation barrier for the formation of an unstable boryl hydride intermediate from a Rh(I) species (cf. **6–13** versus **7–19**, Scheme 11).

Complexes **4** and **5** do not proceed to dehydrocouple, a consequence of the lack of a N–H proton. By contrast, addition of $H_3B \cdot NHMe_2$ to **1** or **3** in $1,2-F_2C_6H_4$ solution results in a more reactive set of complexes which do proceed on to dehydrocouple. Thus, addition of 2 equiv of $H_3B \cdot NHMe_2$ to **1** resulted in an immediate color change to give a short-lived purple complex, characterized by NMR spectroscopy, ESI-MS, and X-ray crystallography as $[Rh(H)_2(\eta^2-H_3B \cdot NHMe_2)(P^iBu_3)_2][BAr^F_4]$ (**6**). **6** proceeds rapidly to give a pale-yellow complex, which has been characterized by NMR spectroscopy, ESI-MS, and X-ray crystallography as $[Rh(H)_2(\eta^2-H_3B \cdot NHMe_2)(P^iBu_3)_2][BAr^F_4]$ (**7**) (Scheme 6). Concomitant with this is the formation of $[H_2BNMe_2]_2$ [$\delta^{(11)B}$ 5.5; $t, J(BH)$ 112 Hz].¹³ Complex **6** thus is an intermediate in the dehydrocoupling of $H_3B \cdot NHMe_2$ with the hydride ligands in the final product **7** presumably coming from the initial dehydrogenation. Addition of smaller amounts (less than 2 equiv) of $H_3B \cdot NHMe_2$ to **1** resulted in the formation of mixtures of **6**, **7**, **2**, and $[H_2BNMe_2]_2$ in varying proportions, meaning that **6** could not be isolated free of **7**. **6** was longer-lived under these conditions allowing for its characterization in solution by ESI-MS and in situ NMR spectroscopy. The NMR data for **6** are very similar

to those found for **4** suggesting a very similar structure, while the NMR data for complex **7** are very close to those observed for **5**.

In solution at room temperature the BH_3 group in complex **7** undergoes rapid exchange between terminal and bridging hydrides that can be frozen out at low temperature (190 K) in contrast to complex **5** where this fluxional process cannot be frozen out at low temperature. At 298 K an integral 3-H signal is observed for the Rh–H–B protons, δ –0.77, and the hydride ligands are observed as a doublet of triplets δ –17.42, displaying cis-coupling to the two equivalent phosphines [$\delta^{(31)P}$ 22.26; $J(RhP)$ 105 Hz]. On cooling (190 K) the fluxional process is halted, and a relative integral 2H signal is observed for the Rh–H–B protons at δ –3.15. The solid-state structure of **7** is shown in Figure 5 and shows a η^2 -coordinated amine–borane on a Rh(III) center, with cis hydrides and trans phosphines. The hydride ligands and BH protons were located in the final electron density difference map. The Rh–B distance, [2.318(8) \AA], is significantly longer than that in **4** reflecting a weaker interaction. It is similar to that observed in $[Rh(cod)(\eta^2-H_3B \cdot PPh_2CH_2PPh_2)][BPh_4]$, [2.313(3) \AA .²⁹ This weaker interaction is mirrored in the ^{11}B NMR chemical shift, δ 2.2 (Table 1). The H1A–Rh1–H1B angle is also more acute [61(3) $^\circ$], reflecting this weaker interaction. The NHMe₂ group is orientated so that the NH proton is directed toward the iBu groups, fitting snugly in a pocket made by the phosphine alkyl groups. This no doubt minimizes steric pressures as the N–H \cdots H–C distances are too long to be considered as strongly attractive, namely, H1 \cdots H3B 2.47; H1 \cdots H7A 2.88 \AA . As with **5**, complex **7** loses H_2 to re-form a Rh(I) complex **6**, but as this

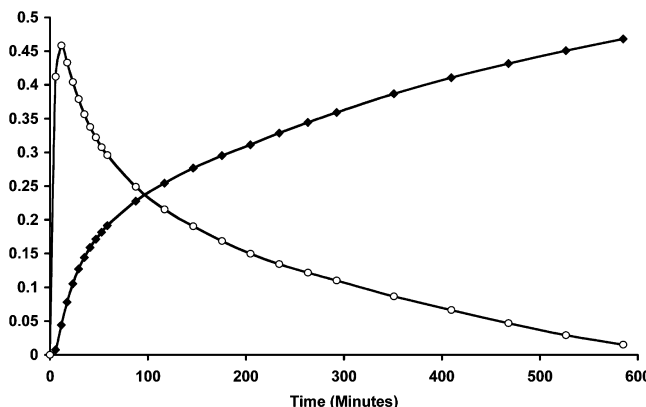


Figure 6. Plot of ^{11}B concentration for the dehydrocoupling of $\text{H}_3\text{B}\cdot\text{NHMe}_2$ (initial concentration = 0.48 mol dm^{-3}) using **1** (298 K , $5 \text{ mol } \%$, $1,2\text{-F}_2\text{C}_6\text{H}_4$, sealed system). \blacklozenge = $[\text{H}_2\text{BNMe}_2]_2$, the final product; \circ = $\text{H}_3\text{B}\cdot\text{NMe}_2\text{BH}_2\cdot\text{NHMe}_2$, **III-Me**. Reaction proceeds to 100% conversion after 600 min.

is unstable itself this eventually results in a mixture of products. The loss of H_2 is much slower, requiring application of a vacuum; this being consistent with the attenuated steric pressure in **7** between the amine–borane and phosphine compared with **5**. Complex **7** can also be accessed by addition of $\text{H}_3\text{B}\cdot\text{NHMe}_2$ to **3**. Addition of $\text{H}_3\text{B}\cdot\text{NHMe}_2$ to $d_2\text{-3}$, $[\text{Rh(D)}_2(\text{P}^{\text{i}}\text{Bu}_3)_2][\text{BAR}^{\text{F}}_4]$, resulted in washing of deuterium to the BH_3 group consistent with a low energy H/D exchange process. DFT optimized structures of **6** and **7** are shown in Section 3 (Figure 16).

Complexes **6** and **7** represent intermediates on the dehydrogenation cycle of $\text{H}_3\text{B}\cdot\text{NHMe}_2$, and **4** and **5** are model complexes for this cycle. All are accessed via addition of the precursor amine–borane to **1** in $1,2\text{-F}_2\text{C}_6\text{H}_4$ solution. We next investigated whether these Rh(I) or Rh(III) species turnover in the catalytic dehydrocoupling of $\text{H}_3\text{B}\cdot\text{NHMe}_2$.

2.2. Catalytic Dehydrogenation of $\text{H}_3\text{B}\cdot\text{NHMe}_2$. Isolated complexes **2** and **7** are active catalysts for the dehydrogenation of $\text{H}_3\text{B}\cdot\text{NHMe}_2$. In an open system under Ar the addition of $\text{H}_3\text{B}\cdot\text{NHMe}_2$ to **2** in $1,2\text{-F}_2\text{C}_6\text{H}_4$ solvent results in a modest^{4,8–11,42} overall turnover frequency (35 min, TOF 34 h^{-1} , 298 K , $5 \text{ mol } \%$, 100% conversion) to ultimately afford the cyclic dimer **IV**. One equivalent of H_2 is released during this process (by gas buret). Addition of Hg did not inhibit catalysis. Repeating this reaction in a sealed NMR tube resulted in a lower TOF (10 h, TOF 2 h^{-1}) suggesting inhibition by H_2 released during catalysis, probably by favoring Rh(III) dihydride complex **3** or **7** rather than a Rh(I) species. Under these attenuated conditions a time/concentration plot (Figure 6) showed no evidence of sigmoidal kinetics, which coupled with the lack of inhibition on addition of Hg suggests nanoparticle formation is not occurring during catalysis.¹² A small amount of $\text{H}_2\text{B}=\text{NMe}_2$, $\delta 38 [\text{d}, J(\text{BH}) 123 \text{ Hz}]^{14}$ was observed during catalysis that followed a time/concentration profile consistent with an intermediate. $\text{H}_2\text{B}=\text{NMe}_2$ can arise from initial dehydrogenation of $\text{H}_3\text{B}\cdot\text{NHMe}_2$ or, as we demonstrate later, also from the dehydrocoupling reaction of **III-Me**. Small amounts (less than 5%) of other amine–boranes are also observed including $\text{HB}(\text{NMe}_2)_2^{57}$ and $(\text{BH}_2)\text{NMe}_2(\mu\text{-H})^{58}$. Using a catalyst loading of 2.5 mol % dehydrocoupling proceeded at a considerably slower rate (80 h, TOF 0.5 h^{-1} , sealed system, see Supporting Information) but still to completion.

Another species that shows characteristic intermediate time/concentration dependence is also observed by ^{11}B NMR spectroscopy in both the open and the closed systems, $\delta 2.5 [\text{t},$

$J(\text{BH}) 112]$, Figures 6 and 7. In our original communication we tentatively identified this as $[\text{H}_2\text{BNMe}_2]_3$,⁴³ on the basis of previous suggestions that this cyclic species is as an intermediate in the dehydrogenation of $\text{H}_3\text{B}\cdot\text{NHMe}_2$ by “ $\text{Cp}_2\text{Ti}''^3$ and Cu/ Ni-N -heterocyclic carbenes.¹¹ This cyclic trimer would be required to undergo B–N bond cleavage to eventually form **IV**, which must be catalyzed, presumably by a transition metal, as $[\text{H}_2\text{BNMe}_2]_3$ has been reported to be stable at least up to its melting point of 97° in the absence of a metal.⁵⁹ However, we now suggest that this intermediate is, in fact, the linear diborazane $\text{H}_3\text{B}\cdot\text{NMe}_2\text{BH}_2\cdot\text{NHMe}_2$, **III-Me**. This linear dimer was first isolated in low yield by Hahn and Schaeffer⁶⁰ and the crystal structure reported by Nöth.⁶¹ An improved synthesis by Manners and co-workers has recently been reported.¹³ In addition they demonstrated that **III-Me** undergoes dehydrocoupling to give **IV** using colloidal Rh catalysts, leading to the suggestion that it was a viable intermediate in the conversion of $\text{H}_3\text{B}\cdot\text{NHMe}_2$ to **IV** using a transition metal catalyst. The proto analogue **III-H**, $\text{H}_3\text{B}\cdot\text{NH}_2\text{BH}_2\cdot\text{NH}_3$, has also been calculated as a possible intermediate in hydrogen loss from $\text{H}_3\text{B}\cdot\text{NH}_3$,^{39,40} although calculations on the Ti-catalyzed dehydrocoupling of $\text{H}_3\text{B}\cdot\text{NHMe}_2$ suggest that metal mediated dehydrocoupling of **III-Me** to form **IV** is not occurring.¹⁷ The ^{11}B chemical shifts for independently prepared¹³ **III-Me** in $1,2\text{-F}_2\text{C}_6\text{H}_4$ solvent are observed at $\delta 2.5 [\text{t}, \text{BH}_2, J(\text{BH}) 112 \text{ Hz}]$ and $\delta -12.8 [\text{q}, \text{BH}_3, J(\text{BH}) 95 \text{ Hz}]$, the former being that observed for the intermediate species (Figure 7). The BH_3 resonance of **III-Me** is very close to that for the starting material $\text{H}_3\text{B}\cdot\text{NHMe}_2$ [$\delta -12.8, \text{t}, J(\text{BH}) 98 \text{ Hz}$] in $1,2\text{-F}_2\text{C}_6\text{H}_4$, and this resonance in the ^{11}B NMR spectrum of the catalysis mixture is rather broad (Figure 7) indicating overlapping signals. When the reaction is quenched with MeCN this change in solvent polarity results in a clear separation of these high-field peaks (Supporting Information). The key data that characterizes this intermediate as **III-Me** in $1,2\text{-F}_2\text{C}_6\text{H}_4$ solvent comes from inspection of the ^1H NMR spectra (Figure 8) that show, in addition to $\text{H}_3\text{B}\cdot\text{NHMe}_2$ and **IV**, two resonances that can be attributed to the *N*-methyl groups of **III-Me**, $2.57 (\text{d}, 6\text{H}, \text{NHMe}_2)$, $2.45 (\text{s}, 6\text{H}, \text{NMe}_2)$, and the NH proton $\delta 5.25 (\text{br s}, 1\text{H}, \text{NH})$. These resonances follow the same time/concentration profile as that for the intermediate in the ^{11}B NMR spectrum. These observations show that **III-Me** is formed, rather than the cyclic trimer $[\text{H}_2\text{BNMe}_2]_3$, as an intermediate which then undergoes Rh-mediated dehydrocoupling to form **IV**. We return to this later.

Monitoring the sealed system during catalysis by NMR spectroscopy also identified a number of metal containing species, including **7** (ca. 20%). Other species currently elude definitive identification. Toward the end of catalysis only two compounds are observed: **7** and another that is currently only characterized by solution techniques, which becomes the dominant species after catalysis is complete and the concentration of $\text{H}_3\text{B}\cdot\text{NHMe}_2$ is close to zero. Addition of further $\text{H}_3\text{B}\cdot\text{NHMe}_2$ to these solutions restarts catalysis. $^{31}\text{P}[^1\text{H}]$ NMR spectroscopy for this new complex suggests a Rh(III) center [$J(\text{RhP}) 104 \text{ Hz}$], while ^1H NMR data indicate $2 \times \text{Rh}-\text{H}$ [$\delta -16.43, 2\text{H}$], $2 \times \text{Rh}-\text{H}-\text{B}$ [$\delta -2.11, 2\text{H}$] groups, the latter

(57) Nöth, H.; Vahrenkamp, H. *Chem. Ber.* **1966**, *99*, 1049–67.

(58) Keller, P. C. *J. Am. Chem. Soc.* **1969**, *91*, 1231.

(59) Campbell, G. W.; Johnson, L. *J. Am. Chem. Soc.* **1959**, *81*, 3800–3801.

(60) Hahn, G. A.; Schaeffer, R. *J. Am. Chem. Soc.* **1964**, *86*, 1503–1504.

(61) Nöth, H.; Thomas, S. *Eur. J. Inorg. Chem.* **1999**, 1373–1379.

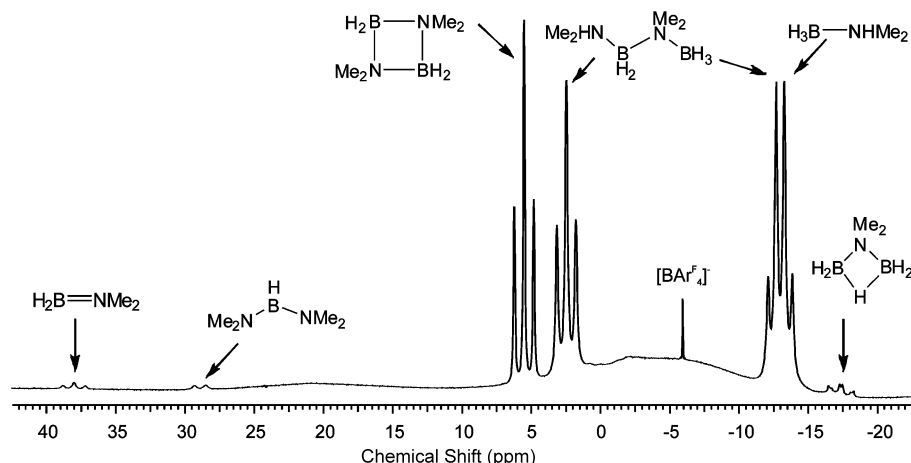


Figure 7. ^{11}B NMR spectrum after 100 min of the catalytic dehydrocoupling of $\text{H}_3\text{B}\cdot\text{NHMe}_2$ using **1** showing the species present. See Figure 6 for more details.

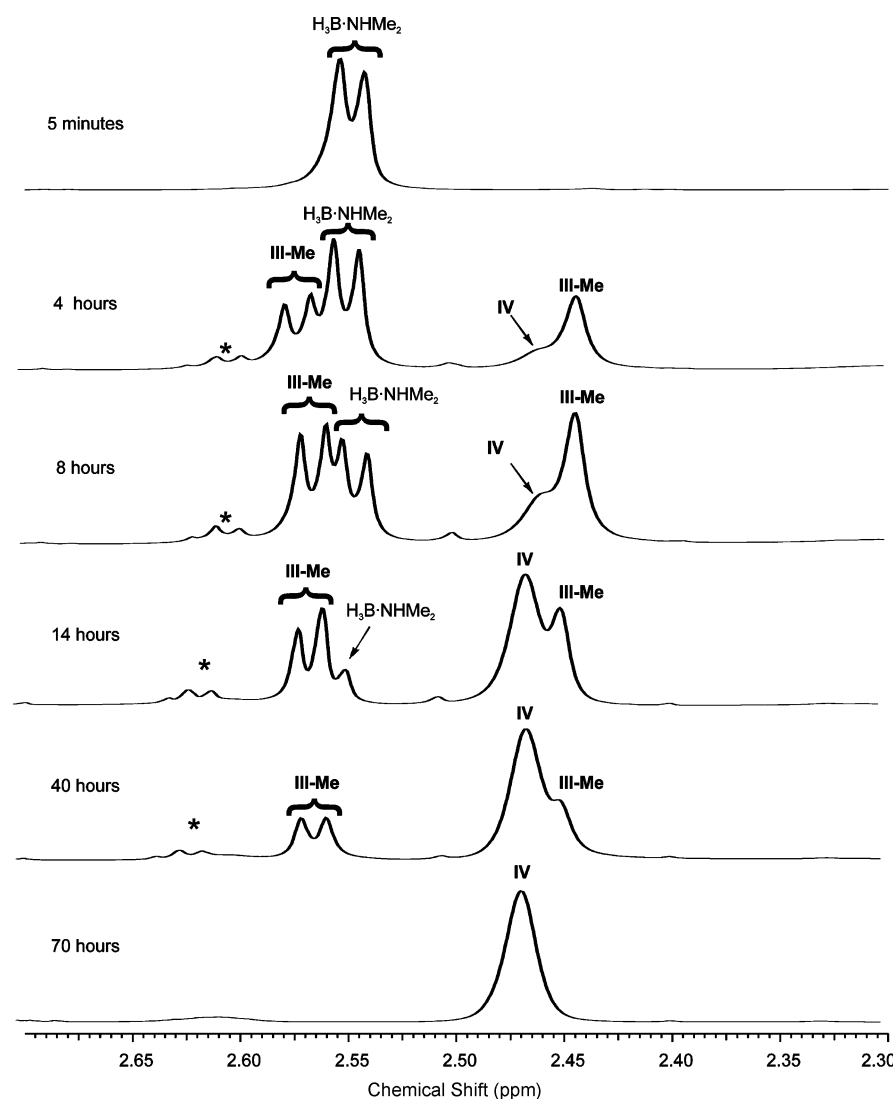


Figure 8. ^1H NMR spectra of the N -methyl region during the catalytic dehydrogenation of $\text{H}_3\text{B}\cdot\text{NHMe}_2$ using **1** (298 K, 2.5 mol %, 1,2- $\text{F}_2\text{C}_6\text{H}_4$, sealed system) over time, showing $\text{H}_3\text{B}\cdot\text{NHMe}_2$, **IV**, and **III-Me**.

also being a nicely resolved 1:1:1:1 quartet [$J(\text{BH})$ 79 Hz] that shows a reduced coupling constant compared to closely related free $\text{H}_2\text{B}=\text{N}^{\text{i}}\text{Pr}_2$ [$J(\text{BH})$ 126 Hz], indicative of a $\text{Rh}^{\bullet}\cdot\text{H}-\text{B}$ interaction.⁵⁵ No NH signals were identified. These data fit an

empirical formula $[\text{Rh}(\text{H})(\text{P}^{\text{i}}\text{Bu}_3)_2(\eta^2-\text{H}_2\text{B}=\text{NMe}_2)]^+$ **8**. We discount assignment as a complex of the product, **IV**, or intermediate, **III-Me**, as independent synthesis of these complexes gives very different NMR spectroscopic signatures (vide

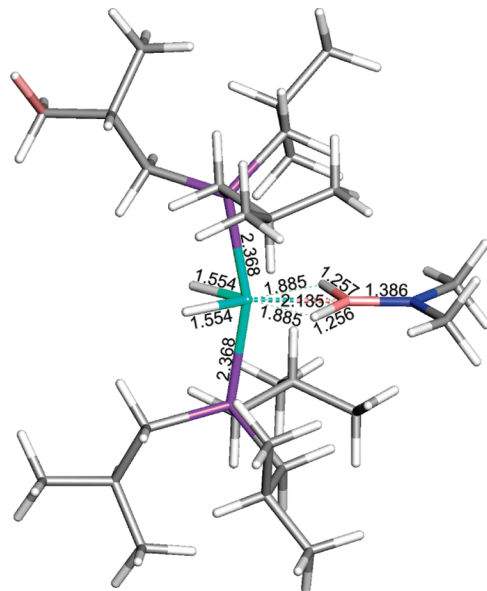


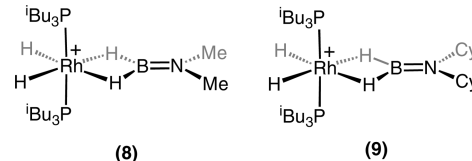
Figure 9. DFT optimized structure of the cationic portion of **8**. Bond lengths in Å.

infra). In support of this assignment, addition of $\text{H}_2\text{B}=\text{NCy}_2$ ⁶² to **1** in 1,2-F₂C₆H₄ solution results in a complex with similar NMR spectroscopic characteristics to **8** that is characterized by NMR spectroscopy as $[\text{Rh}(\text{H})_2(\text{P}^i\text{Bu}_3)_2(\eta^2-\text{H}_2\text{B}=\text{NCy}_2)]^+$ **9**. Despite repeated attempts we have not been able to obtain a crystalline material of this complex. Complex **9** shows a slightly broadened, integral 2-H signal at $\delta = -14.51$ due to the Rh hydrides, and a quadrupolar broadened, integral 2-H signal at $\delta = -1.71$. No N–H signal was observed. The ¹¹B NMR spectrum of **9** shows a very broad resonance at $\delta = 35$, which although essentially unshifted from free amino–borane is significantly broader than free ligand.⁶² We saw no evidence for free amino–borane. Although, as far as we are aware, other complexes of amino–boranes have yet to be reported, complexes of three coordinate mesitylborane have recently been described and show an end on, η^2 -coordination mode for the borane.³⁵ We tentatively also assigned an end-on coordination mode for the amino–borane in **9** as this fits the observed ¹H NMR data and also would minimize steric interactions with the *trans*-phosphine groups. With the less bulky $\text{H}_2\text{B}=\text{NMe}_2$ in **8** a side-on coordination motif might be more accessible. DFT calculations predict that in **8**, whose optimized structure is shown in Figure 9, the ligand $\text{H}_2\text{B}=\text{NMe}_2$ does not coordinate side-on but only end-on through two Rh–H–B bridges. When the iBu_3P ligands were modeled by the sterically smaller Me_3P ligands, a structure with $\text{H}_2\text{B}=\text{NMe}_2$ coordinated side-on to Rh could be determined. However, even for this simplified model, the end-on structure for $\text{H}_2\text{B}=\text{NMe}_2$ is about 15 kcal/mol more stable (see Supporting Information for more details). These results strongly indicate and end-on structures for both **8** and **9** (Scheme 7).

2.3. Synthesis of σ -Complexes of $\text{H}_3\text{B}\cdot\text{NMe}_2\text{BH}_2\cdot\text{NHMe}_2$ and $[\text{H}_2\text{BNMe}_2]_2$. Given that **III-Me** (a postulated intermediate) and the final product of the reaction, **IV**, can both potentially coordinate to a metal center, we have investigated the independent synthesis of complexes of these two amine–boranes with the $[\text{Rh}(\text{P}^i\text{Bu}_3)_2]^+$ fragment.

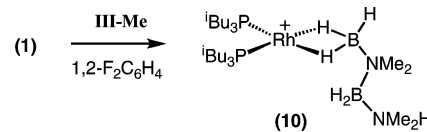
(62) Euzenat, L.; Horvant, D.; Ribourdouille, Y.; Duriez, C.; Alcaraz, G.; Vaultier, M. *Chem. Commun.* **2003**, 2280–2281.

Scheme 7. Comparison of the Proposed Structures of **8** and **9**^a



^a $[\text{BAr}^F_4]^-$ anions are not shown.

Scheme 8. Synthesis of **10**^a



^a $[\text{BAr}^F_4]^-$ anions are not shown.

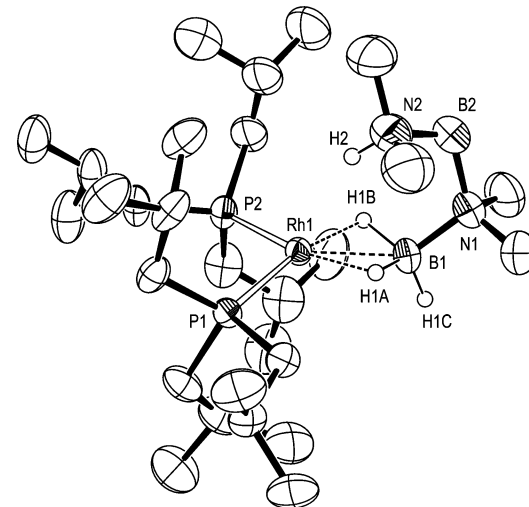


Figure 10. Molecular structure the cationic portion of **10**: ellipsoids depicted at the 50% probably level. Only one of the independent molecules in the asymmetric unit is shown; most H atoms omitted for clarity. Selected bond lengths (Å) and angles (deg): Rh1–B1, 2.166(8); Rh1–P1, 2.243(2); Rh1–P2, 2.248(2); B1–N1, 1.565(11); N1–B2, 1.588(14); B2–N2, 1.621(14); Rh1–H1A, 1.74(3); Rh1–H1B, 1.74(3); Rh1–H2, 2.54; Rh1–N2, 3.89(8); B1–H1A, 1.30(3); B1–H1B, 1.30(3); B1–H1C, 1.09(6); P1–Rh1–P2, 99.19(6); P1–Rh1–B1, 130.3(3); P2–Rh1–B1, 128.2(3); Rh1–B1–N1, 134.3(7); B1–N1–B2, 116.0(7); N1–B2–N2, 114.4(8); Rh1–H1A–B1, 90.2; Rh1–H1B–B1, 90.2; H1A–Rh1–H1B, 72(2); Rh1–H2–N2, 152.2; H2 in calculated position.

Using the same synthetic route as for the previous complexes, addition of **III-Me** to a 1,2-F₂C₆H₄ solution of **2** gives immediate and quantitative formation (by NMR spectroscopy) of $[\text{Rh}(\text{P}^i\text{Bu}_3)_2(\eta^2-\text{H}_3\text{B}\cdot\text{NMe}_2\text{BH}_2\cdot\text{NHMe}_2)][\text{BAr}^F_4]$ **10** (Scheme 8). In our hands complex **10** is very air-sensitive in the solid and solution state and consequently difficult to isolate and purify. Temperature-sensitive crystalline material was grown at –30 °C. The hydrogen atoms associated with the Rh–H–B interaction were located in the final Fourier difference map, which show the borane to be η^2 -bound to the metal center in the solid-state structure (Figure 10). DFT calculations support their positioning (Figure 11), as does NMR spectroscopy.

In the solid state, complex **10** crystallizes with two independent molecules in the asymmetric unit, with similar structural metrics for both (see Supporting Information). **III-Me** binds to the Rh(I) metal center via two B–H–Rh 3c–2e bonds and has similar structural metrics to those observed for **4** (and **12**, vide infra) and chelated η^2 -phosphine borane complexes of Rh(I).²⁹

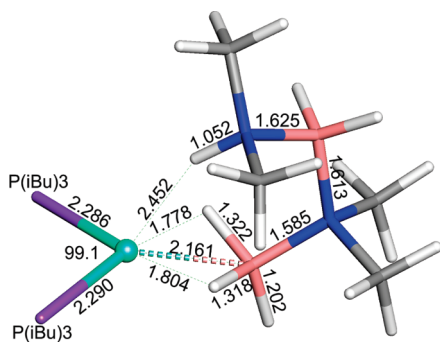


Figure 11. DFT optimized structure of the cationic portion of **10**. Bond lengths in Å. Bond angle in degrees. The ^tBu groups are not shown for clarity.

The Rh(I) is pseudo-square planar coordinated, with a rather short Rh \cdots B distance [2.166(8)/2.202(9) Å], similar to that found in **4**. There appears to be a close interaction between N–H₂ and the Rh [e.g., 2.54 Å, 152°] and although not linear, it is still probably best described as a 3c–4e Rh \cdots H–N hydrogen bond.⁶³ This interaction in **10** could represent an early stage in the process of H-transfer to the metal—a mechanistic step in the dehydrocoupling. Interestingly there is also a gradual shortening of the B–N bonds as they become closer to the metal center [1.565(11)/1.546(12)–1.621(14)/1.593(12) Å], unlike in parent **III-Me** where they are all essentially the same [1.589(2)–1.600(2) Å].⁶¹ In solution (1,2-F₂C₆H₄) at room temperature the BH₃ group is observed as a broad, integral 3 H signal at δ –2.31, demonstrating rapid exchange between terminal and bridging hydrides. The BH₂ group is not observed, presumably obscured by the aliphatic peaks. The BH₃ resonances are shifted upfield from that of observed free ligand, consistent with coordination of the metal. The NH proton is observed at δ 4.31 [cf. free ligand δ 5.45]. The ¹¹B{¹H} NMR spectrum shows two broad resonances at δ 26.0 and δ 3.9, the former assigned to the BH₃ group, and is shifted by 38.8 ppm downfield [viz. 2.5 (BH₂), –12.8 (BH₃) in **III-Me**]. Although the ¹¹B resonances are too broad to observe multiplicity in the coupled spectrum which would aid assignment, selective decoupling of the δ 26.0 peak results in a sharpening of the δ –2.31 resonance in the ¹H NMR spectrum, identifying it as the BH₃ signal. The ³¹P{¹H} NMR spectrum shows a single resonance with a large [J (RhP) 173 Hz] coupling constant, consistent with a Rh(I) center. ESI-MS shows a parent ion at m/z = 623.444 (calcd 623.441). Cooling a CH₂Cl₂ solution of **2** to 200 K halts the fluxional process that exchanges the terminal B–H protons on B1 so that an integral 2H, Rh–H–B, signal is now observed at δ –5.93 in the ¹H NMR spectrum. The corresponding terminal B–H resonance was not observed. The N–H bond is unshifted. These NMR data are fully consistent with the solid-state structure.

Interestingly in 1,2-F₂C₆H₄ solution complex **10** does not undergo further dehydrocoupling to form the cyclic oligomer **IV**, being stable for 24 h in solution. This shows that **10** does not proceed to dehydrocouple to give **IV** via a simple intramolecular route. In support of a more complex process, addition of two equivalents of **III-Me** to **1** in 1,2-F₂C₆H₄ solution results in the immediate formation of a number of organometallic products: **7** (10%), **10** (50%), and a new complex tentatively identified by NMR spectroscopy and ESI-MS as [Rh(H)₂(η^2 -

H₃B \cdot NMe₂BH₂ \cdot NHMe₂)(P*i*Bu₃)₂][BAr^F₄] **11** (40%). Leaving this mixture for a further 2 h resulted in a change in composition to **11** (35%) and **7** (65%) together with the formation of **IV**. The NMR spectra of **11** show signals due to Rh–H–B (δ –0.75, 2H) and Rh–H [δ –18.60, 2H, apparent quartet (dt, J 20 Hz)] and a single ³¹P environment [δ 21.5, J (RhP) 107 Hz] with a chemical shift and coupling constant similar to those of **5** and **7**. Definitive signals due to **11** could not be assigned in the ¹¹B NMR spectrum. ESI-MS shows a strong molecular ion at m/z = 625.457 in full accord with the formulation as a dihydride (Figure 12). Although the mechanism of dehydrocoupling for **III-Me** thus appears to be less than straightforward, most importantly these observations demonstrate that **III-Me** and transition metal complexes thereof are plausible intermediates on the dehydrocoupling pathway, underscoring the previous experimental observations by Manners as well as our observation here that **III-Me** is an intermediate. The observation of **7**, however, suggests that B–N bond cleavage has occurred during the dehydrocoupling process, and this perhaps points to a complicated and possibly multipathway process that might invoke intermolecular activation. Indeed, computational studies on the dehydrogenation of H₃B \cdot NH₃ suggest that the related linear dimer H₃N \cdot BH₂NH₂ \cdot BH₃ is formed that then proceeds via production of 2 equiv of H₂B=NH₂ and H₂, the former which then reacts with H₃B \cdot NH₃ in an autocatalytic reaction.³⁹ The metal-catalyzed dehydrogenation was not investigated in this study. For **III-Me**, separate computational studies suggest an off-metal dehydrogenation mechanism involves a relatively high barrier (29.9 kcal mol^{–1}) and production of 2 equiv of Me₂B=NH₂ alongside H₂.¹⁷

Under catalytic conditions in a sealed NMR tube **10** and **2** are effective, but not spectacular, catalysts, for the dehydrocoupling of **III-Me** (5 mol %, 1,2-F₂C₆H₄, sealed system, 70 h, TOF 0.3 h^{–1}) to form **IV** (Figure 13), a comparable rate to that observed for the overall dehydrogenation of H₃B \cdot NHMe₂ (2.5 mol %) under the same conditions (Supporting Information). These data suggest that dehydrocoupling of **III-Me** is the rate determining processes in the overall dehydrogenation of H₃B \cdot NHMe₂. Approximately 1 equiv of H₂ per **III-Me** is evolved during this catalytic process (gas buret). H₂B=NH₂ is also formed during catalysis, suggesting a mechanism that involves B–N cleavage as one pathway, adding further support for B–N bond cleavage in the dehydrocoupling of the **III-Me** under stoichiometric conditions.

Addition of **IV** to **3** is followed by immediate H₂ loss and the isolation deep-purple [Rh(P*i*Bu₃)₂{ η^2 -(H₂BNMe₂)₂}][BAr^F₄] **12** (Scheme 9) as the only product. Alternatively **12** can be prepared by addition of **IV** to **1** in 1,2-F₂C₆H₄. The solid-state structure is shown in Figure 14 and shows a η^2 -coordination motif for the cyclic borane, similar to that observed for **4** and **10**. **12** crystallizes as two independent salts in the asymmetric unit cell, but there is no significant variation between the two discrete sets of molecules. The BH hydrogen atoms associated with B1 were located. The Rh \cdots B distances, [2.161(6)/2.140(7) Å], are comparable with that in **4** and **10**. There appears to be no major change in bond lengths and angles in [H₂BNMe₂]₂ compared to the free ligand,¹³ although B–N bond lengths associated with B1 are slightly shorter than those with B2 or those found in the free ligand by \sim 0.05 Å. The sum of angles around Rh1 come to 360°. DFT calculations are in close accord with the experimentally determined structure (Figure 15).

In solution the [H₂BNMe₂]₂ ligand is static on the metal center, and two BH₂ environments are observed in the ¹H

(63) Brammer, L. *Dalton Trans.* 2003, 3145–3157.

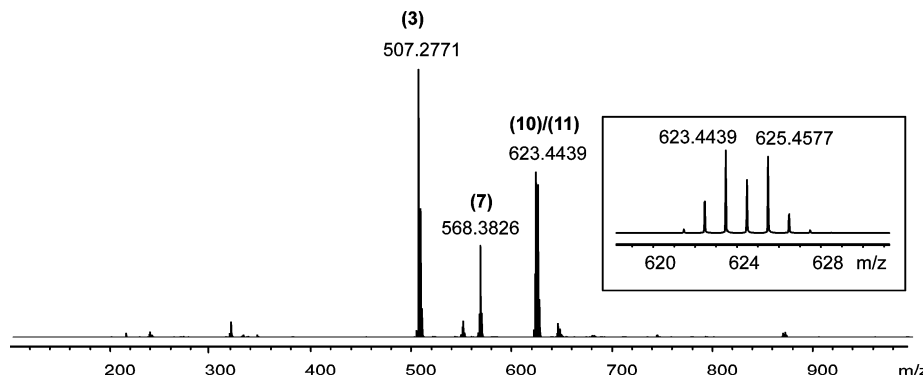


Figure 12. ESI-MS of the addition of 2 equiv of **III-Me** to **1**. Inset expands the 618–631 region. Complex **3** is not observed in the reaction mixture by NMR spectroscopy and arises from loss of amine–borane from **7**, **10**, and **11** under the conditions of ESI-MS.

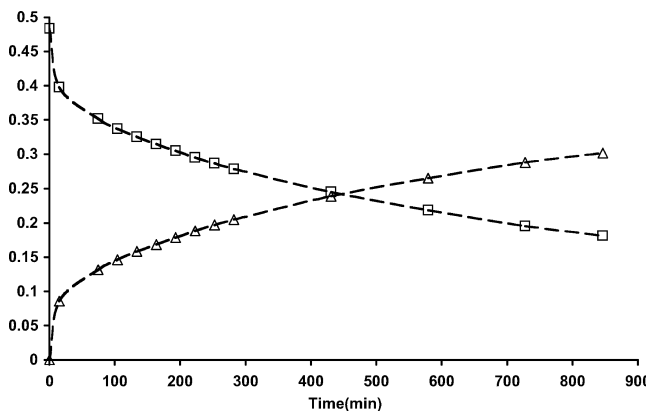
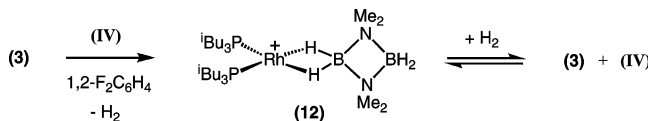


Figure 13. Concentration plot for the dehydrocoupling of **III-Me** (initial concentration = 0.48 mol dm⁻³) using **1** (298 K, 5 mol %, 1,2-F₂C₆H₄, sealed system). □ = **III-Me**, △ = **IV**.

Scheme 9. Synthesis of Complex **12**^a



^a [BAr₄^F]⁻ anion is not shown.

NMR spectrum. One is interacting with the metal, δ –5.07 [quartet, $J(BH)$ 89 Hz], while the other is not, δ 2.90 [vbr]. The reduced coupling constant in the higher-field signal compared to free ligand [cf. 112 Hz] is consistent with σ -coordination of the B–H bond with the metal center.^{21,55} The ¹¹B NMR spectrum also shows two environments (δ 31.1, 5.4), and selective ¹H{¹¹B} experiments show that the one at δ 31.1 is due to the η^2 borane, is shifted 25.7 ppm downfield from free ligand, and also shows a reduced coupling constant, [$J(HB)$ 89 Hz],¹³ while the other is unshifted, δ 5.4 [vbr], and assigned to B2. Complex **12** comes from addition of **IV** to **3** and H₂ loss, this presumably occurring due to steric pressure between the *trans* phosphine ligands and the borane in the Rh(III)-dihydride, as found for **5** and **7**. With no conformational flexibility available to [H₂B(NMe₂)₂] the resulting dihydride species is clearly too unstable to isolate. Addition of H₂ to a 1,2-F₂C₆H₄ solution of **12** results in an equilibrium mixture of **12** and **3/IV**, consistent with this idea. Removal of the H₂ atmosphere re-established **12**.

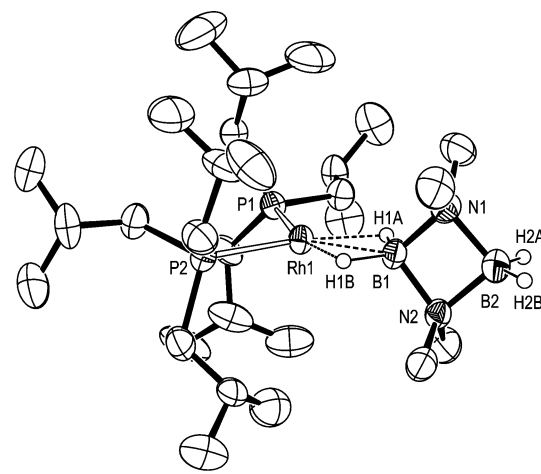


Figure 14. Molecular structure of the cationic portion of **12**: ellipsoids depicted at the 50% probably level. One of the independent molecules in the asymmetric unit; minor disordered component and most H atoms omitted for clarity. Selected bond lengths (Å) and angles (deg): Rh1–B1, 2.161(6); Rh1–P1, 2.2457(14); Rh1–P2, 2.253(2); B1–N1, 1.559(8); B1–N2, 1.547(8); B2–N1, 1.596(9); B2–N2, 1.605(9); Rh1–H1A 1.87(5); Rh1–H1B 1.69(5); B1–H1A 1.21(3); B1–H1B 1.21(3); B2–H2A 1.09(3); B2–H2B 1.09(3); P1–Rh1–P2, 98.31(6); P1–Rh1–B1, 130.9(2); P2–Rh1–B1, 130.8(2); N1–B1–N2, 94.6(4); N1–B2–N2, 91.0(5); B1–N2–B2, 86.5(4); B1–N1–B2, 86.4(4); Rh1–H1A–B1, 87(3); Rh1–H1B–B1, 95(3); H1A–Rh1–H1B, 68(2).

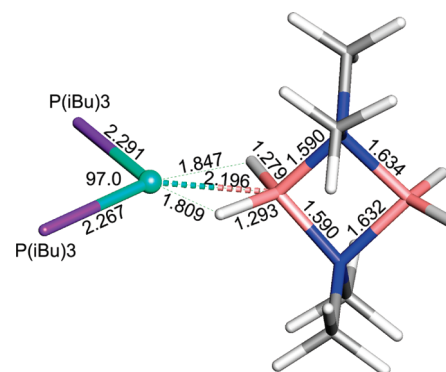
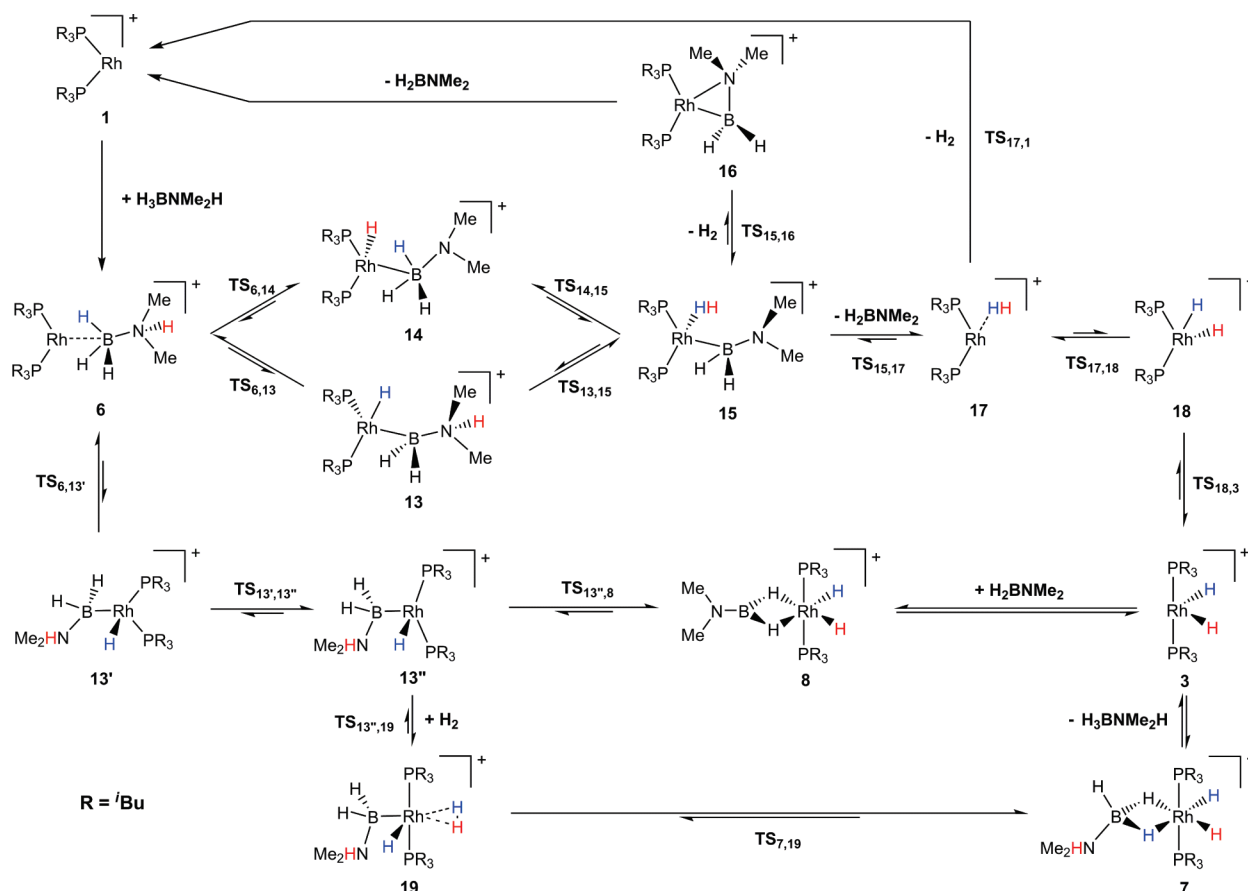


Figure 15. DFT optimized structure of the cationic portion of **12**. Bond lengths in Å. Bond angle in degrees. The ⁱBu groups are not shown for clarity.

3. Computational Study

With intermediates and model complexes in hand we now turn to computational techniques to help elucidate possible mechanistic

Scheme 10. Proposed Reaction Mechanism for the Dehydrogenation of $H_3B \cdot NMe_2H$ Using **1**

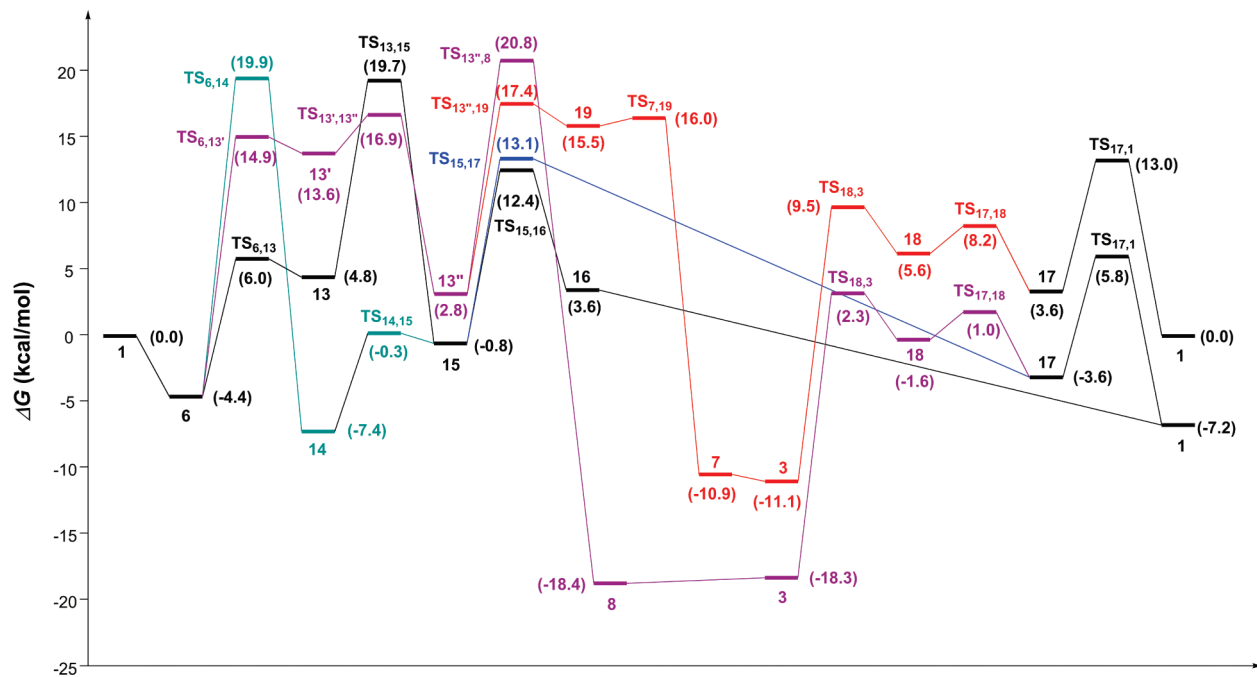
pathways for the dehydrocoupling reaction using catalyst **1**. This study has been limited to the first proposed dehydrogenation step of $H_3B \cdot NMe_2H$ to afford $H_2B=NMe_2$ given the potential complexity (e.g., linear dimer formation, B–N bond cleavage reactions) of the subsequent dehydrogenation steps to afford **IV**. Although in $1,2\text{-F}_2C_6H_4$ solution **2** is the organometallic precatalyst, the study starts from 12-electron **1** (Figure 1) as the first step in any mechanistic pathway is likely to be dissociation of the bound arene solvent from this 18-electron complex. Schemes 10 and 11 shows these sequential processes and give a free-energy profile for the intrinsic reaction coordinate. Figure 16 shows the structure of the selected intermediates. Supporting Information give geometries for all the calculated structures reported here.

The initial dehydrogenation of $H_3B \cdot NMe_2H$ has been investigated by following possible pathways that involve NH/BH or BH/NH activation. Calculations indicate that there are two competitive pathways that begin with the formation of the σ -complex **6** and then bifurcate by either N–H or B–H bond activation. $Rh(P{^i}Bu_3)_2$ reacts with $H_3B \cdot NMe_2H$ to instantly form the adduct **6**, which is bound by -4.4 kcal/mol in solvent corrected free-energy. H-transfer to the Rh center then occurs either through B–H bond activation, transition state **TS_{6,13}**, or through N–H bond activation, transition state **TS_{6,14}**, to form intermediate **13** or **14**, respectively. Although **14** is 12.2 kcal/mol lower than **13** in free energy, the barrier to NH transfer (**TS_{6,14}**) is much higher than BH oxidative addition (**TS_{6,13}**): 24.3 vs 10.4 kcal/mol, respectively. The second H transfer to Rh occurs either from the nitrogen in **13** or from the boron in **14**, proceeding through transition states **TS_{13,15}** or **TS_{14,15}** respectively to afford the Rh(I)/dihydrogen intermediate **15**, the largest barrier in this instance being **TS_{13,15}** (14.9 kcal/mol). In this catalytic dehydrocoupling cycle of $H_3B \cdot NMe_2H$ to afford metal bound $H_2B=NMe_2$ the rate determining steps are two N–H bond activation transition states **TS_{6,14}** and **TS_{13,15}**, which are at essentially the same overall solvent corrected free energy, thus making both

pathways competitive with one another. An alternate higher energy BH/NH bond activation pathway is discussed later.

The second part of the mechanistic pathway follows from **15** and requires H_2 loss from the metal in **15**. This has been studied by following two possible pathways. For the first, dihydrogen in **15** can be released through transition state **TS_{15,16}** with a barrier of 13.2 kcal mol $^{-1}$. Simultaneous to this release, the N atom is attracted by Rh to form intermediate **16**, with the $H_2B=NMe_2$ ligand bonding with the Rh(I) center through a three-center, two-electron Rh–H–B bridging interaction and a weak Rh–N bond (2.281 Å). Catalyst **1** is then regenerated by release of $H_2B=NMe_2$ from **16**. Alternatively, instead of H_2 release from **15**, $H_2B=NMe_2$ can be released through transition state **TS_{15,17}**, which is only 0.7 kcal/mol higher than **TS_{15,16}** in free energy to form intermediate **17**, which contains a dihydrogen ligand. H_2 loss from this regenerates **1**. This close match in calculated energy mean that pathways are equally accessible in practice. The **TS_{16,1}** and **TS_{8,3}** (vide infra) could not be determined. These ligand dissociation transition states are often problematic to determine as the location of the transition state along the reaction coordinate is poorly defined. However, based on the somewhat similar **TS_{15,17}**, these barriers are estimated to be about 14 kcal/mol.

An alternative, productive, dehydrocoupling pathway involves initial oxidative addition of the B–H bond, to ultimately give an alternate isomer to **13**, **13''** (**TS_{6,13'}** 19.3 kcal/mol), in which the phosphine ligands are orientated significantly wider apart and more trans-like than in **13**, in which they are cis. This leads to an intermediate almost isoenergetic with **13** but one that can now proceed in a very different pathway to **13**. N–H transfer from **13''** leads to **8** with a reasonable barrier of 18.0 kcal/mol (**TS_{13'',8}**) which has an end-on coordination mode of $H_2B=NMe_2$ and lies in a deep potential-energy well. This then proceeds via loss of $H_2B=NMe_2$ to give **3** that then moves through **18** to give **17** via reductive bond formation, followed by H_2 loss to finally regenerate **1**. The

Scheme 11. Solvent Effect Corrected Free Energy Reaction Profile^a

^a Refer to Scheme 10 and Supporting Information for the structures of the intermediates. The final energies of **1** differ as the pathway through **7** does not involve dehydrogenation of H₃B•NMe₂H.

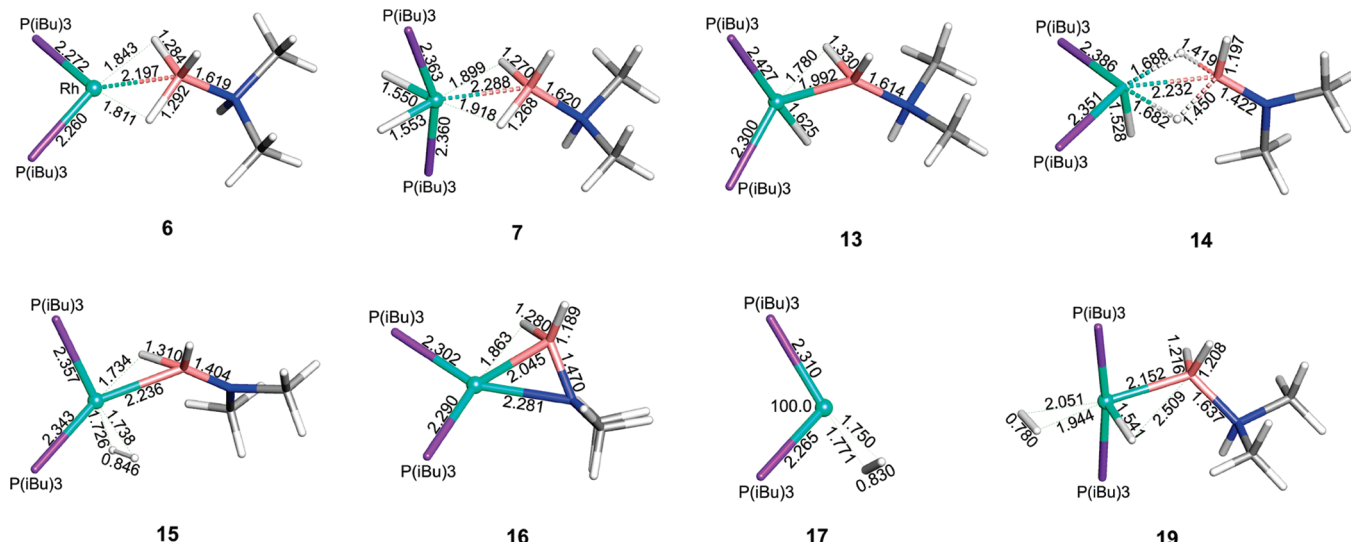


Figure 16. Optimized geometric structures of the cationic portions of intermediates **6**, **7**, **13**, **14**, **15**, **16**, **17**, and **19**. Bond lengths in Å. The ⁱBu groups are not shown for clarity.

transformation of **3** to **18** is an isomerization (TS_{18,3} 20.6 kcal/mol), with **3** 16.7 kcal/mol more favorable than **18**; as when the geometries are compared, **18** has a weaker Rh–H bond trans to the Rh–P bond and a more acute P–Rh–P angle that results in larger steric repulsions between the phosphines. The highest barrier to this overall process is TS_{18,3} (20.6 kcal/mol) followed closely by a step early in the reaction coordinate TS_{6,13'} 19.3 kcal/mol. Both of these are large but accessible. That **8** sits in such a deep well but also has a relatively high barrier to access suggests that it will pool slowly during catalysis and be a major, thermodynamically favored product at the end. This is observed experimentally. That **8** can also be formed from **3** mirrors the synthetic route to form **9**.

Complex **7** can be accessed via **13''** by H₂ addition to give **19** which has a dihydrogen and base-stabilized borylene ligand. Concerted H₂ cleavage and B–H bond formation leads to **7**. The

largest barrier to this is TS_{13'',19}, 14.6 kcal/mol, which leads to **7** that sits in a relatively deep well (although not as deep as **8**). These energies fit with the experimental observation that **7** is observed during catalysis but will eventually be disfavored with respect to **8** at low substrate concentrations and long reaction times. The pathway **1** to **7** to **1** via **19** is not a productive dehydrogenation step, as overall it is simply addition and loss of H₃B•NMe₂H and H₂. However, complex **7** does lie on a productive pathway as defined by **7**–**19**–**13''**–**8**–**3**–**7**, but as **7**–**19** is particularly high energy (26.9 kcal/mol), this is not a kinetically significant process on the basis of these calculations.

Overall these calculations suggest that initial activation of H₃B•NMe₂H to form metal-bound H₂B=NMe₂ occurs either via BH oxidative addition/NH transfer or NH activation/BH transfer. This is followed by sequential H₂ loss/H₂B=NMe₂ loss or sequential H₂B=NMe₂ loss/H₂ loss. These dissociation pathways have very

similar calculated barriers, which are also close to the NH activation barrier, suggesting that on the bench these competing pathways are all energetically accessible. The pooling of **8** at the end of the reaction, and **7** being observed during catalysis, sits with the relative calculated thermodynamic stabilities of these complexes and the reversibility of their formation, especially **7**. The stepwise pathway for dehydrogenation is similar (although the order different) to that proposed for titanocene systems¹⁷ but different from the concerted mechanism using Ir-pincer complexes that invokes a Ir(III)/Ir(V) process.¹⁸

4. Conclusions

We have reported a combined experimental/quantum chemical investigation of the dehydrocoupling reaction of $H_3B \cdot NMe_2H$ to ultimately give the cyclic dimer $[H_2BNMe_2]_2$. Intermediates and model complexes have been isolated, including examples of amine–borane σ -complexes of Rh(I) and Rh(III), and for the first time the isolation of a transition metal complex of the oligomeric dimer $H_3B \cdot NMe_2BH_2 \cdot NHMe_2$, which has been shown to be an intermediate in the dehydrocoupling reaction. DFT calculations show that the first proposed dehydrogenation step, to give $H_2B=NMe_2$, proceeds via sequential BH/NH activation followed by two possible routes that invoke sequential H_2 loss/ $H_2B=NMe_2$ loss or $H_2B=NMe_2$ loss/ H_2 loss. For the second dehydrogenation step that ultimately affords $[H_2BNMe_2]_2$ the experimental observation that the isolated and crystallographically characterized complex $[Rh(P^iBu_3)_2(\eta^2-H_3B \cdot NMe_2BH_2 \cdot NHMe_2)][BAr^F_4]$ is stable in the absence of added amine–borane suggests that a simple intramolecular route for this dehydrocoupling process is not operating for this linear dimer. Although the catalysts reported here demonstrate rather poor turnover frequencies, it is exactly because of this that intermediates can be observed and isolated under stoichiometric conditions. Future studies will address the influence that the phosphine and identity of the metal has on both the rate of catalysis and the intermediates observed in the anticipation of providing yet more information on this important transformation.

5. Experimental Section

All manipulations, unless otherwise stated, were performed under an atmosphere of argon, using standard Schlenk and glovebox techniques. Glassware was oven-dried at 130 °C overnight and flamed under vacuum prior to use. Pentane was dried using a Grubbs type solvent purification system (MBraun SPS-800) and degassed by successive freeze–pump–thaw cycles.⁶⁴ CD_2Cl_2 and 1,2-F₂C₆H₄ were distilled under vacuum from CaH₂ and stored over 3 Å molecular sieves. Na[BAr^F₄],⁶⁵ [Rh(nbd)(PⁱBu₃)₂][BAr^F₄],⁴⁶ [Rh(PⁱBu₃)₂][BAr^F₄] (**1**),⁴⁶ [Rh(H)₂(PⁱBu₃)₂][BAr^F₄] (**4**),⁴⁶ $[H_2BNMe_2]_2$,¹³ $H_2B=N$ Cy₂,⁶² and $H_3B \cdot NMe_2BH_2 \cdot NHMe_2$ ¹³ were prepared by published literature methods or variations thereof. NMR spectra were recorded on Varian 500 MHz and Bruker 500 MHz spectrometers. Difluorobenzene (center of downfield multiplet) was used as reference for ¹H NMR spectra (1,2-F₂C₆H₄: δ = 7.07). ³¹P NMR spectra were referenced against 85% H₃PO₄ (external). ¹¹B NMR spectra were referenced against BF₃·OEt₂ (external). Chemical shifts are quoted in ppm and coupling constants in Hz. ESI-MS were recorded on a Bruker MicroOTOF-Q instrument.⁶⁶ The correct isotope patterns were observed for all species reported, as modeled by the Bruker MicroOTOF software. Microanalyses were

performed by Elemental Microanalysis Ltd. $H_3B \cdot NMe_3$ and $H_3B \cdot NHMe_2$ were purchased from Aldrich and sublimed twice before use (5×10^{-2} Torr, 298 K). pcq = partially collapsed quartet. All ¹¹B NMR spectra show a singlet at ca. δ = 6.0 due to the [BAr^F₄]⁻ anion.

Chemical Shifts of Previously Reported Amine–Boranes in 1,2-F₂C₆H₄ (298 K). $H_3B \cdot NMe_3$. ¹H NMR (500 MHz, 1,2-F₂C₆H₄): δ 2.27 [q, 3 H, BH₃, J(BH) 98], 2.63 (s, 9 H, NMe). ¹¹B{¹H} NMR (160 MHz, 1,2-F₂C₆H₄, 298 K): δ = 7.3 [q, J(BH) 98].

$H_3B \cdot NHMe_2$. ¹H NMR (500 MHz, 1,2-F₂C₆H₄) δ 3.87 (s, 1H, Br, NH), 2.55 [d, 6 H, NMe, J(HH) 5], 2.13 [pcq, 3 H, BH₃, J(BH) 96]. ¹¹B{¹H} NMR (160 MHz, 1,2-F₂C₆H₄, 298 K): δ = 12.8 [q, J(BH) 96].

$H_3B \cdot NMe_2BH_2 \cdot NHMe_2$.¹³ ¹H NMR (500 MHz, 1,2-F₂C₆H₄): δ 5.45 (s, 1H, NH), 2.55 [d, 6 H, NMeH, J(HH) 6], 2.45 [s, 6 H, NMe], 2.16 [pcq, 2 H, BH₂, J(BH) 107], 2.04 [pcq, 3 H, BH₃, J(BH) 94]. ¹¹B NMR (160 MHz, 1,2-F₂C₆H₄, 298 K): δ 2.5 [t, BH₂, J(BH) 107], −12.8 [q, BH₃, J(BH) 94].

$[H_2BNMe_2]_2$.¹³ ¹H NMR (500 MHz, 1,2-F₂C₆H₄): δ 2.48 (s, 12 H, NMe), 2.97 [q, 4 H, BH₂, J(BH) 112]. ¹¹B{¹H} NMR (160 MHz, 1,2-F₂C₆H₄, 298 K): δ 5.5 [t, J(BH) 112].

[Rh(η^6 -1,2-F₂C₆H₄)(PⁱBu₃)₂][BAr^F₄] (2). [Rh(PⁱBu₃)₂][BAr^F₄] (30 mg, 2.19×10^{-2} mmol) was dissolved in 1,2-F₂C₆H₄ (2 cm³) to give [Rh(η^6 -1,2-F₂C₆H₄)(PⁱBu₃)₂][BAr^F₄] as an orange solution. Single crystals of **2** were obtained by diffusion of pentane into the solution of **2** (22 mg, 68% yield). **2** was characterized by NMR spectroscopy and ESI-MS in 1,2-F₂C₆H₄ solution. Dissolving crystals of **2** in C₂H₄Cl₂ gave [Rh(C₂H₄Cl₂)(PⁱBu₃)₂][BAr^F₄] and free 1,2-F₂C₆H₄.

¹H NMR (500 MHz, 1,2-F₂C₆H₄): δ 8.34 (s, 8H, BAr^F₄), 7.69 (s, 4H, BAr^F₄), 2.02 (m, 6H, ⁱBu CH), 1.65 (m, 12H, ⁱBu CH₂), 1.13 [d, J(HH) 6, 36H, CH₃]. ³¹P{¹H} NMR (202 MHz, 1,2-F₂C₆H₄): δ 25.91 [d, J(RhP) 210]. ESI-MS (CH₂Cl₂, 100 °C) positive ion {Rh(PⁱBu₃)₂}⁺: *m/z* = 507.28 [M]⁺ (calcd 507.28).

[Rh(η^2 -H₃B·NMe₃)(PⁱBu₃)₂][BAr^F₄] (4). Addition of $H_3B \cdot NMe_3$ (5 mg, 6.8×10^{-2} mmol, 2 equiv) to a solution of **1** (45 mg, 3.2×10^{-2} mmol) in 1,2-F₂C₆H₄ (1 cm³) resulted in a rapid color change from orange to deep purple; diffusion of pentane into the solution gave **4** as dark purple crystals (40 mg, 87%).

¹H NMR (500 MHz, 1,2-F₂C₆H₄, 298 K): δ 8.33 (s, 8H, BAr^F₄), 7.69 (s, 4H, BAr^F₄), 2.96 (s, 9H, N—CH₃), 2.17 (br, 6H, CH), 1.79 (br, 12H, CH₂), 1.24 [d, J(HH) 6, 36H, CH₃], −2.12 (br, 3H, BH₃). ³¹P{¹H} NMR (202 MHz, 1,2-F₂C₆H₄, 298 K): δ 35.94 [d, J(RhP) 175]. ¹¹B{¹H} NMR (160 MHz, 1,2-F₂C₆H₄, 298 K): δ 23.12 (br). Selected ¹³C{¹H} NMR (126 MHz, CD₂Cl₂, 298 K): 53.37 (s, N—CH₃), 39.45 (apparent t, *J* 13, P—CH₂), 26.85 (m, CH), 25.60 (s, CH₃). Selected ¹H NMR (500 MHz, CD₂Cl₂, 190 K): δ = −5.55 (vbr, 2H, η -BH₂), the other BH signal was not observed, presumably as it was broad and obscured by the aliphatic resonances. ESI-MS (1,2-F₂C₆H₄, 100 °C, 4.5 kV): *m/z* = 580.388 (calcd for [C₂₇H₆₆BNP₂Rh]⁺ 580.382). Microanalysis (C₅₉H₇₈B₂F₂₄NP₂Rh, 1443.71 g mol^{−1}): requires, C, 49.09; H, 5.45; N, 0.97.; found, C, 48.92; H, 5.25; N, 1.02.

[Rh(H)₂(η^2 -H₃B·NMe₃)(PⁱBu₃)₂][BAr^F₄] (5). Addition of H_2 (4 atm, 298 K/77 K = 3.8) to a solution of [Rh(H)₂B·NMe₃](PⁱBu₃)₂][BAr^F₄] (10 mg, 6.9×10^{-3} mmol) in 1,2-F₂C₆H₄ (0.3 cm³) resulted in a rapid color change from deep purple to pale yellow. **5** was characterized *in situ* by NMR spectroscopy. Attempts to obtain crystalline material of **6** were unsuccessful due to facile H_2 loss to give **4**. ¹H and ³¹P{¹H} NMR spectra showed no change on cooling to 190 K. ESI-MS showed only a peak corresponding to **4** [*m/z* = 580.38]. **5** could also be prepared by addition of TMAB to a solution of **3** in 1,2-F₂C₆H₄.

¹H NMR (500 MHz, 1,2-F₂C₆H₄, 298 K): δ 8.33 (s, 8H, BAr^F₄), 7.69 (s, 4H, BAr^F₄), 2.87 (s, 9H, N—CH₃), 2.08 (br, 6H, CH), 1.83 (br, 12H, CH₂), 1.14 [d, J(HH) 6, 36H, CH₃], −0.47 (br, 3H, BH₃), −18.81 [dt, J(RhH) 23, J(PH) 17, 2H, Rh—H]. ³¹P{¹H} NMR (202 MHz, 1,2-F₂C₆H₄, 298 K): δ 21.10 [d, J(RhP) 106]. ¹¹B{¹H} NMR

- (64) Pangborn, A. B.; Giardello, M. A.; Grubbs, R. H.; Rosen, R. K.; Timmers, F. J. *Organometallics* **1996**, *15*, 1518–1520.
 (65) Buschmann, W. E.; Miller, J. S.; Bowman-James, K.; Miller, C. N. *Inorg. Synth.* **2002**, *33*, 83–85.
 (66) Lubben, A. T.; McIndoe, J. S.; Weller, A. S. *Organometallics* **2008**, *27*, 3303–3306.

(160 MHz, 1,2-F₂C₆H₄, 298 K): δ 5.07 (br). Selected ¹³C{¹H} NMR (126 MHz, CD₂Cl₂, 298 K): 56.52 (s, N—CH₃), 39.05 (m, P—CH₂), 26.61 (m, CH), 25.37 (s, CH₃).

[Rh(η^2 -H₃B•NHMe₂)(P*i*Bu₃)₂][BAr^F₄] (6). Addition of H₃B•NHMe₂ (0.196 M in 1,2-F₂C₆H₄, 37 μ L, 7.3 \times 10⁻³ mmol, 1 equiv) to a solution of **1** (10 mg, 7.3 \times 10⁻³ mmol) in 1,2-F₂C₆H₄ (1 cm³) resulted in a rapid color change from orange to deep purple. **6** was characterized in situ by NMR spectroscopy and ESI-MS. **6** rapidly (10 min) decomposes in solution to give **6** and other unidentified products. Addition of more than 1 equiv of H₃B•NHMe₂ results in much shorter lived **6** and the observation of dimeric [H₂BNMe₂]₂.

¹H NMR (500 MHz, 1,2-F₂C₆H₄, 298 K): δ 8.33 (s, 8H, BAr^F₄), 7.69 (s, 4H, BAr^F₄), 4.67 (br, 1H, NH), 2.88 (s, 6H, N—CH₃), 2.07 (br, 6H, CH), 1.79 (br, 12H, CH₂), 1.19 (m, 36H, CH₃), -2.13 (br, 3H, BH₃). ³¹P{¹H} NMR (202 MHz, 1,2-F₂C₆H₄, 298 K): δ 35.9 [d, *J*(RhP) 174]. ¹¹B{¹H} NMR (160 MHz, 1,2-F₂C₆H₄, 298 K): δ 19.31 (br). ESI-MS (1,2-F₂C₆H₄, 100 °C, 4.5 kV): *m/z* = 566.366 (calcd for [C₂₆H₆₄BNP₂Rh]⁺ 566.369).

[Rh(H)₂(η^2 -H₃B•NHMe₂)(P*i*Bu₃)₂][BAr^F₄] (7). Addition of H₃B•NHMe₂ (0.406 M in 1,2-F₂C₆H₄, 36 μ L, 1.4 \times 10⁻² mmol, 2 equiv) to a solution of **1** (10 mg, 7.3 \times 10⁻³ mmol) in 1,2-F₂C₆H₄ (0.3 cm³) gave [Rh(H)₂(P*i*Bu₃)₂(H₃B•NHMe₂)][BAr^F₄] (**7**) as a pale yellow solution which was characterized in situ by NMR spectroscopy and ESI-MS. Concomitant with the formation of **7**, [H₂BNMe₂]₂ was also observed. A single crystal suitable for X-ray diffraction studies was obtained by diffusion of pentane into a 1,2-F₂C₆H₄ solution at -35 °C.

¹H NMR (500 MHz, 1,2-F₂C₆H₄, 298 K): δ 8.43 (s, 8H, BAr^F₄), 7.79 (s, 4H, BAr^F₄), 3.87 (s, 1H, NH), 2.97 (s, 6H, N—CH₃), 2.17 (br, 6H, CH), 1.91 (br, 12H, CH₂), 1.24 [d, *J*(HH) 6, 36H, CH₃], -0.77 (br, 3H, BH₃), -17.42 [dt, *J*(RhH) 19.5, *J*(PH) 17.3, 2H, Rh—H]. ³¹P{¹H} NMR (202 MHz, 1,2-F₂C₆H₄, 298 K): δ 22.26 [d, *J*(RhP) 105]. ¹¹B{¹H} NMR (160 MHz, 1,2-F₂C₆H₄, 298 K): δ 2.23 (br). Selected ¹H NMR (500 MHz, CD₂Cl₂, 190 K): δ -3.15 (vbr, 2H, η -BH₂), the other BH signal was not observed, presumably as it was broad and obscured by the aliphatic resonances. ESI-MS (1,2-F₂C₆H₄, 100 °C, 4.5 kV): *m/z* = 568.385 (calcd for [C₂₆H₆₆BNP₂Rh]⁺ 568.382).

[Rh(H)₂(H₂B=NCy₂)(P*i*Bu₃)₂][BAr^F₄] (9). Addition of H₂ (4 atm, 298 K/77 K = 3.8) to a solution of [Rh(nbd)(P*i*Bu₃)₂][BAr^F₄] (10 mg, 6.8 \times 10⁻³ mmol) in 1,2-F₂C₆H₄ (0.3 mL) gave **3** as a pale yellow solution. H₂B=NCy₂ (0.25 M in 1,2-F₂C₆H₄, 28 μ L, 7.0 \times 10⁻³ mmol, 1 equiv) was added and the resulting solution characterized in situ by NMR spectroscopy and ESI-MS. Attempts to isolate crystalline material of **9** suitable for microanalysis or X-ray crystallography have failed to afford suitable material for analysis.

¹H NMR (500 MHz, 1,2-F₂C₆H₄, 298 K): δ 8.83 (s, 8H, BAr^F₄), 7.69 (s, 4H, BAr^F₄), 3.22 (m, 2H, N—CH), 2.50–0.79 (m, 38H, CH₂/CH), 1.15 [d, *J*(HH) 6, 36H, CH₃], -1.71 (br, 2H, BH₂), -14.51 (br, 2H, Rh—H). ³¹P{¹H} NMR (202 MHz, 1,2-F₂C₆H₄, 298 K): δ 22.36 [d, *J*(RhP) 99]. ¹¹B NMR (160 MHz, 1,2-F₂C₆H₄, 298 K): δ 35 (vbr). ESI-MS (1,2-F₂C₆H₄, 100 °C, 4.5 kV): *m/z* = 702.485 (calcd for [C₃₆H₈₀BNP₂Rh]⁺ 702.491).

[Rh(H₃B•NMe₂BH₂•NHMe₂)(P*i*Bu₃)₂][BAr^F₄] (10). Addition of H₃B•NMe₂BH₂•NHMe₂ (2.5 mg, 2.19 \times 10⁻² mmol) to a 1,2-F₂C₆H₄ (1 cm³) solution of **1** (30 mg, 2.19 \times 10⁻² mmol) resulted in a rapid color change from orange to deep purple. In situ NMR spectroscopy demonstrated complete conversion to **10**. Diffusion of pentane into the 1,2-F₂C₆H₄ solution at -35 °C gave [Rh(H₃B•NMe₂BH₂•NHMe₂)(P*i*Bu₃)₂][BAr^F₄] as dark red crystals (25 mg, 77%).

¹H NMR (500 MHz, 1,2-F₂C₆H₄, 298 K) δ 8.33 (s, 8H, BAr^F₄), 7.69 (s, 4H, BAr^F₄), 4.31 (br s, 1H, NH), 2.70 (d, 6H, N—CH₃), 2.64 (s, 6H, N—CH₃), 2.19 (m, 6H, CH), 1.77 (m, 12H, CH₂), 1.23 [d, *J*(HH) 6.7, 36H, CH₃], -2.31 (br s, 3H, BH₃). The BH₂ signal could not be assigned. ³¹P{¹H} NMR (121.51 MHz, 1,2-F₂C₆H₄, 298 K): δ 37.46 [d, *J*(RhP) 173 Hz]. ¹¹B{¹H} NMR (160.40 MHz, 1,2-F₂C₆H₄, 298 K): δ 26.04 (br s), 3.89 (v br s). Selected ¹H NMR

(500.13 MHz, CD₂Cl₂, 190 K): δ -5.93 (br s, 2H, σ -BH), the remaining BH and BH₂ signals were not observed, presumably obscured under aliphatic resonances. ESI MS (1,2-F₂C₆H₄, 100 °C, 4.5 kV): *m/z* = 623.444 (calcd for [RhC₂H₇₂P₂B₂N₂]⁺ 623.441).

[Rh(H)₂(η^2 -H₃B•NMe₂BH₂•NHMe₂)(P*i*Bu₃)₂][BAr^F₄] (11). Addition of H₃B•NMe₂BH₂•NHMe₂ (0.033 M in 1,2-F₂C₆H₄, 0.22 cm³, 7.3 \times 10⁻³ mmol, 1 equiv) to a 1,2-F₂C₆H₄ (0.5 cm³) solution of [Rh(P*i*Bu₃)₂][BAr^F₄] (10 mg, 7.29 \times 10⁻³ mmol) resulted in a rapid color change from orange to purple. The solution was immediately characterized in situ by NMR spectroscopy and shown to contain a mixture of [Rh(η^2 -H₃B•NMe₂BH₂•NHMe₂)(P*i*Bu₃)₂][BAr^F₄] (**10**) (50%), [Rh(H)₂(η^2 -H₃B•NMe₂BH₂•NHMe₂)(P*i*Bu₃)₂][BAr^F₄] (**11**) (40%) and [Rh(H)₂(η^2 -H₃B•NMe₂BH₂•NHMe₂)(P*i*Bu₃)₂][BAr^F₄] (**7**) (10%). Leaving for 2 h resulted in observation of **7** (65%) and **11** (35%) by NMR spectroscopy. [H₂BNMe₂]₂ is also observed to be formed.

¹H NMR (500 MHz, 1,2-F₂C₆H₄, 298 K): δ 8.33 (s, 8H, BAr^F₄), 7.69 (s, 4H, BAr^F₄), 4.24 (br s, 1H, NH), 2.78 (m, 6H, N—CH₃), 2.58 (s, 6H, N—CH₃), 2.07 (m, 6H, CH), 1.81 (m, 12H, CH₂), 1.13 [d, *J*(HH) 6.7, 36H, CH₃], -0.75 (br s, 3H, BH₃), -18.60 [apparent quartet, *J* 20, 2H, Rh—H]. BH₂ signal could not be assigned as it is probably obscured by the aliphatic resonances. ³¹P{¹H} NMR (121.51 MHz, 1,2-F₂C₆H₄, 298 K): δ 21.50 [d, *J*(RhP) 107 Hz]. ¹¹B{¹H} NMR (160.40 MHz, 1,2-F₂C₆H₄, 298 K): could not be assigned, too broad. ESI MS (1,2-F₂C₆H₄, 100 °C, 4.5 kV): *m/z* = 625.457 (calcd for [RhC₂H₇₂P₂B₂N₂]⁺ 625.4). Also observed are **10** [*m/z* = 623.444] and **7** [*m/z* = 580.38] in approximately the same ratio as in the solution NMR spectroscopy experiment.

[Rh(P*i*Bu₃)₂{ η^2 -(H₂BNMe₂)₂}][BAr^F₄] (12). Addition of [H₂BNMe₂]₂ (5 mg, 4.4 \times 10⁻² mmol, 3 equiv) to a solution of **1** (20 mg, 1.5 \times 10⁻² mmol) in 1,2-F₂C₆H₄ (1 cm³) resulted in a rapid color change from orange to deep purple. NMR spectroscopy showed that the reaction was quantitative. Diffusion of pentane into the solution gave **12** as deep purple crystals (11 mg, 51%). Addition of H₂ (4 atm, 298 K/77 K = 3.8) to a solution of **12** in 1,2-F₂C₆H₄ gave a mixture of **3**, **12**, and [H₂BNMe₂]₂. Removal of the H₂ atmosphere re-established complex **12**.

¹H NMR (500 MHz, 1,2-F₂C₆H₄, 298 K): δ 8.33 (s, 8H, BAr^F₄), 7.69 (s, 4H, BAr^F₄), 2.90 (vbr, 2H, BH₂), 2.69 (s, 12H, N—CH₃), 2.18 (m, 6H, CH), 1.84 (m, 12H, CH₂), 1.27 [d, *J*(HH) 6, 36H, CH₃], -5.07 (q, *J*(BH) 89, 2H, Rh—H₂B). BH assignments based on ¹H{¹¹B-selective} experiments. ¹³³¹P{¹H} NMR (202 MHz, 1,2-F₂C₆H₄, 298 K): δ 33.38 [d, *J*(RhP) 170]. ¹¹B NMR (160 MHz, 1,2-F₂C₆H₄, 298 K): δ 31.14 [t, *J*(BH) 88, 1B, Rh—H₂B], 5.36 (vbr, 1B, BH₂). ESI-MS (1,2-F₂C₆H₄, 100 °C, 4.5 kV): *m/z* = 621.419 (calcd for [C₂₈H₈₀B₂N₂P₂Rh]⁺ 621.426). Microanalysis (C₆₀H₈₂B₃F₄N₂P₂Rh): requires, C, 48.54; H, 5.57; N, 1.89; found, C, 48.43; H, 5.62; N, 1.79.

Reactions of [Rh(D)₂(P*i*Bu₃)₂][BAr^F₄] with H₃BN•HMe₂ and H₃B•NMe₂. [Rh(nbd)(P*i*Bu₃)₂][BAr^F₄] (10 mg, 6.84 \times 10⁻³ mmol) was placed under D₂ (4 atm) to give [Rh(D)₂(P*i*Bu₃)₂][BAr^F₄] as a pale yellow solution which was characterized in situ by NMR spectroscopy. Excess H₃B•NMe₂ (1 mg) was added to the solution of [Rh(D)₂(P*i*Bu₃)₂][BAr^F₄] and monitored in situ by ¹H NMR spectroscopy. Initially a broad signal at approximately δ -0.6 consistent with coordinated BH₃ was observed and no high field hydride signals. Over 10 min the BH₃ signals reduce in intensity with the concomitant appearance of high field hydride signals at approximately δ -18, H₂ at δ 4.60, and HD at δ 4.56 *J*(HD) 42 Hz. The coordination of D₃B•NMe₂ was confirmed by ESI-MS. ESI-MS calcd for [RhP₂C₂₇H₆₃D₃P₂B₁N₁]⁺ 583.401, obsvd; 583.406, calcd.

Excess H₃B•NHMe₂ (1 mg) was added to the solution of [Rh(D)₂(P*i*Bu₃)₂][BAr^F₄] and monitored in situ by ¹H NMR spectroscopy. A broad signal at approximately δ -0.6 consistent with coordinated BH₃, hydride signals at approximately δ -18, H₂ at δ 4.60, and HD at δ 4.56 [*J*(HD) 42 Hz] were all observed.

Catalytic Dehydrocoupling of H₃B•NHMe₂ with **1 in a Sealed NMR Tube.** In a typical experiment H₃B•NHMe₂ (8.6 mg, 1.5 \times 10⁻¹ mmol, 20 equiv) and **1** (10 mg, 7.3 \times 10⁻³ mmol)

Table 2. Crystallographic Data

	2^a	4	7	10	12
formula	C ₆₂ H ₇₀ BF ₂₆ P ₂ Rh	C ₅₉ H ₇₈ B ₂ F ₂₄ NP ₂ Rh	C ₅₈ H ₇₈ B ₂ F ₂₄ NP ₂ Rh	C ₆₀ H ₈₄ B ₃ F ₂₄ N ₂ P ₂ Rh	C ₆₀ H ₈₂ B ₃ F ₂₄ NP ₂ Rh
<i>M</i>	1484.84	1443.69	1431.68	1486.57	1484.56
cryst syst	monoclinic	monoclinic	monoclinic	orthorhombic	monoclinic
space group	<i>P</i> 2 ₁ / <i>n</i>	<i>P</i> 2 ₁ / <i>c</i>	<i>C</i> 2/ <i>c</i>	<i>Pna</i> 2 ₁	<i>P</i> 2 ₁ / <i>n</i>
<i>a</i> [Å]	21.7964(2)	12.97140(10)	21.0042(3)	50.6131(4)	14.2225(2)
<i>b</i> [Å]	13.1712(2)	20.0178(2)	18.2723(3)	19.6787(2)	50.9939(7)
<i>c</i> [Å]	25.5387(3)	26.8437(2)	37.9197(7)	14.39940(10)	19.5840(3)
β [deg]	113.7594(5)	93.4556(1)	102.2898(6)		91.5253(7)
<i>V</i> [Å ³]	6710.37(14)	6957.53(10)	14219.9(4)	14341.8(2)	14198.5(4)
<i>Z</i>	4	4	8	8 (<i>Z'</i> = 2)	8 (<i>Z'</i> = 2)
density [g cm ⁻³]	1.470	1.378	1.337	1.377	1.389
μ (mm ⁻¹)	0.412	0.391	0.382	0.382	0.386
θ range [deg]	5.10 $\leq \theta \leq$ 26.37	5.14 $\leq \theta \leq$ 25.03	5.10 $\leq \theta \leq$ 25.03	5.14 $\leq \theta \leq$ 25.03	5.12 $\leq \theta \leq$ 25.03
reflns collected	13607	23229	20424	19425	22815
<i>R</i> _{int}	0.0540	0.0175	0.0638	0.0228	0.075
no. of data/restr/param	13607/1596/1207	12157/111/911	12085/13/863	19425/1564/2004	22815/470/1997
<i>R</i> ₁ , <i>wR</i> ₂ [<i>I</i> > 2σ(<i>I</i>)]	0.0906, 0.2499	0.0542, 0.1387	0.0862, 0.1909	0.0563, 0.1357	0.0685, 0.1284
GoF	1.023	1.020	1.038	1.076	1.093
flack <i>x</i>				0.48(3)	
largest diff. peak and hole [e Å ⁻³]	2.089, ^b -0.958	0.672, -0.536	0.826, -0.762	0.989, -0.446	1.373, ^c -0.606

^a This is a low quality solution and is only included to show the gross structure. ^b With the exception of one Fourier peak (2.089 eÅ⁻³) at 1.74 Å from Rh1, attributed to Fourier truncation errors, the max residual density peak is 1.48 eÅ⁻³. ^c With the exception of one Fourier peak (1.37 eÅ⁻³) at 1.47 Å from Rh1, attributed to Fourier truncation errors, the max residual density peak is 0.62 eÅ⁻³.

were placed into a New Era high pressure NMR sample tube. 1,2-F₂C₆H₄ (0.3 mL) was added by vacuum transfer. The reaction was followed immediately in situ by ¹¹B{¹H} NMR spectroscopy. Under these conditions the reaction went to completion by ¹¹B NMR spectroscopy and gave two metal containing species, **7** and a complex characterized in situ and tentatively assigned as [Rh(H)₂(H₂B=NMe₂)(PⁱBu₃)₂][BAR^F₄] **8** by comparison with complex **9**. Selected ¹H NMR (500 MHz, 1,2-F₂C₆H₄, 298 K): δ -2.11 [bs q, *J*(BH) 79, 2H, BH₂], -16.43 (br, 2H, Rh—H). ³¹P{¹H} NMR (202 MHz, 1,2-F₂C₆H₄, 298 K): δ 18.97 [d, *J*(RhP) 104]. As a result of the low relative concentration of **8** in the catalysis mixture we were unable to assign a ¹¹B resonance to complex **8**.

Catalytic Dehydrocoupling of H₃B•NHMe₂ with **1 in an Open System.** In a typical experiment H₃B•NHMe₂ (0.196 M in 1,2-F₂C₆H₄, 0.75 mL, 0.146 mmol, 20 equiv) was added to a stirred sample of **1** (10 mg, 7.3 × 10⁻³ mmol) in a Schlenk flask open to an argon atmosphere. The 50 μL samples were taken after 5, 15, and 35 min. Samples were diluted with 1,2-F₂C₆H₄, frozen, and analyzed by ¹¹B NMR spectroscopy immediately following warming to RT. Complete conversion to [H₂BNMe₂]₂ was achieved within 35 min, as measured by ¹¹B NMR. Under the same conditions no change in rate was observed when mercury (0.1 mL) was added to the reaction mixture. Addition of H₃B•NHMe₂ (8.6 mg, 1.5 × 10⁻¹ mmol, 20 equiv) to the postcatalysis mixture resulted in the onset of catalysis; complete conversion to [H₂BNMe₂]₂ was again achieved within 35 min. Following the reaction by hydrogen loss using a water-filled gas-burrette showed that approximately 1 equiv of H₂ is lost per H₃B•NHMe₂.

Catalytic Dehydrocoupling of III-Me. In a typical experiment **III-Me** (17 mg, 1.5 × 10⁻¹ mmol, 20 equiv) and **1** (10 mg, 7.3 × 10⁻³ mmol) were placed into a New Era high pressure NMR sample tube. 1,2-C₆H₄F₂ (0.3 mL) was added by vacuum transfer. The reaction was followed in situ by ¹¹B{¹H} NMR spectroscopy at 298 K. Under these conditions the reaction gave **IV** in quantitative yield in 70 h.

X-ray Crystallography. Relevant details about the structure refinements are given in Table 2. As all crystals were extremely air-sensitive they were placed in dried and degassed perfluoropolyalkylether (viscosity 1600 cSt, ABCR) in a glovebox and then mounted rapidly under a stream of argon. Data were collected on an Enraf Nonius Kappa CCD diffractometer using graphite monochromated Mo K α radiation (λ = 0.71073 Å) and a low-temperature

device [150(2) K];⁶⁷ data were collected using COLLECT, and reduction and cell refinement was performed using DENZO/SCALEPACK. Structures were solved by direct methods using SIR92 (**7**, **12**)⁶⁸ and SIR2004 (**4**, **9**, **10**)⁶⁹ and refined full-matrix least-squares on *F*² using SHELXL-97.⁷⁰ All non-hydrogen atoms were refined anisotropically. H0a and H0b in **7** were located on the Fourier difference map and their position refined freely (isotropic displacement parameters were fixed to ride on Rh1). BH protons in all compounds were located on the Fourier difference map (isotropic displacement parameters were fixed to ride on the parent B atoms), with the exception of those on B2 and B12 in **10**. Restraints to BH bonds were applied as follows: B1—H1A = B1—H1B in **4** and **7** (B1—H1C free to refine); B1—H1A = B1—H1B = B11—H11A = B11—H11B, Rh1—H1A = Rh1—H1B = Rh2—H11A = Rh2—H11B, B1—H1C = B11—H11C, H1A…H1C = H1B…H1C, H11A…H11C = H11B…H11C in **10**; B1—H1A = B1—H1B = B3—H3A = B3—H3B, B2—H2A = B2—H2B = B4—H4A = B4—H4B, H2A…H2B = H4A…H4B in **12**. All other hydrogen atoms were placed in calculated positions using the riding model. Excessive thermal motion of some of the phosphine ligands was treated by modeling the relevant phosphine substituents over two sites and restraining their geometries. Rotational disorder of CF₃ groups on the anions was present in all of the structures. The relevant fluorine atoms were modeled over two sites, and the geometries restrained were necessary. Problematic solvent disorder in the solution of **7** was treated using the SQUEEZE algorithm.⁷¹ Restraints to the thermal parameters were applied where necessary to maintain sensible values. Graphical representations of the structures were made with XP⁷⁰ and ORTEP3.⁷²

Computational Details. All density functional theory calculations in this study were performed using the Gaussian 03 suite of ab initio programs⁷³ with the nonempirical Tao-Perdew-Staroverov-

- (67) Cosier, J.; Glazer, A. M. *J. Appl. Crystallogr.* **1986**, *19*, 105–107.
- (68) Altomare, A.; Cascarano, G.; Giacovazzo, C.; Guagliardi, A. *J. Appl. Crystallogr.* **1993**, *26*, 343–350.
- (69) Burla, M. C.; Caliandro, R.; Camalli, M.; Carrozzini, B.; Cascarano, G. L.; De Caro, L.; Giacovazzo, C.; Polidor, G.; Spagna, R. *J. Appl. Crystallogr.* **2005**, *38*, 381–388.
- (70) Sheldrick, G. M. *Acta Crystallogr., Sect. A* **2008**, *64*, 112–122.
- (71) Spek, A. L. *J. Appl. Crystallogr.* **2003**, *36*, 7–13.
- (72) Farrugia, L. *J. Appl. Crystallogr.* **1997**, *30*, 565–565.
- (73) Frisch, M. J.; et al. *Gaussian 03*, Revision E.01; Gaussian, Inc.: Wallingford, CT, 2004 (suite of programs for ab initio calculation).

Scuseria⁷⁴ (TPSS) functional and with the all-electron basis set 6-31G(d,p)⁷⁵ (Def2-TZVP with ECP basis set for Rh).⁷⁶ The geometric structures of all complexes studied in this paper were optimized as gas-phase as the cation only. Calculating the harmonic vibrational frequencies at the optimized structures and noting the number of imaginary frequencies confirmed the nature of all intermediates (no imaginary frequency) and transition states (only one imaginary frequency), which also were confirmed to connect reactants and products by the intrinsic reaction coordinate (IRC) calculations. The zero-point energy (ZPE) and entropic contribution have been estimated within the harmonic potential approximation. The enthalpies, H , and free energies, G , were calculated for $T = 298.15\text{ K}$. All relative energies are reported in kcal/mol. The effect of solvent was taken into account by single point calculations on gas-phase optimized structures using the integral equation formalism polarizable continuum model (IEFPCM) for chlorobenzene ($\epsilon = 5.621$ as a mimic of the 1,2-F₂C₆H₄ solvent). The figures for optimized 3D molecular structures displayed in text are drawn by using the JIMP2 molecular visualization and manipulation program.⁷⁷

- (74) Tao, J. M.; Perdew, J. P.; Staroverov, V. N.; Scuseria, G. E. *Phys. Rev. Lett.* **2003**, *91*, 146401.
- (75) (a) Hehre, W. J.; Ditchfield, R.; Pople, J. A. *J. Chem. Phys.* **1972**, *56*, 2257–2261. (b) Franci, M. M.; Pietro, W. J.; Hehre, W. J.; Binkley, J. S.; Gordon, M. S.; DeFrees, D. J.; Pople, J. A. *J. Chem. Phys.* **1982**, *77*, 3654–3665.
- (76) (a) Weigend, F.; Ahlrichs, R. *Phys. Chem. Chem. Phys.* **2005**, *7*, 3297. (b) Andrae, D.; Haeussermann, U.; Dolg, M.; Stoll, H.; Preuss, H. *Theor. Chim. Acta* **1990**, *77*, 123.

Acknowledgment. This work was supported by Grants from NSF (CHE-0518074, CHE-0541587, and DMS-0216275), The Welch Foundation (A0648), the EPSRC (EP/E050743/1), and the University of Oxford. Mr. Romaeo Dallanegra (Oxford) is thanked for the low temperature NMR spectrum of **10**. Dr. Simon Aldridge (Oxford) is thanked for stimulating discussions and the gift of H₂B=NCy₂.

Note Added after ASAP Publication. Errors were present in the caption to Figure 13 and the last sentence of the first paragraph of the Experimental Section in the version published ASAP September 28, 2009. The corrected version was published October 1, 2009.

Supporting Information Available: Reactivity of **2** with ClCH₂CH₂Cl. Details of crystallographic analysis for the new compounds. Plot of ¹¹B concentration for the dehydrocoupling of H₃B•NHMe₂ using **2** and MeCN-quenching experiment. Complete reference 73, 3D molecular structures, atomic coordinates, and absolute energies of all optimized stationary points and transition states. This material is available free of charge via the Internet at <http://pubs.acs.org>.

JA906070R

- (77) (a) Hall, M. B.; Fenske, R. F. *Inorg. Chem.* **1972**, *11*, 768. (b) Manson, J.; Webster, C. E.; Hall, M. B. *JIMP2*, version 0.091; Texas A&M University: College Station, 2006 (a free program for visualizing and manipulating molecules).